Genome-wide phage susceptibility analysis in *Acinetobacter baumannii* reveals capsule modulation strategies that determine phage infectivity

Jinna Bai[a], Nicole Raustad[a], Jason Denoncourt[a], Tim van Opijnen[b], Edward Geisinger[a]#

[a]Department of Biology, Northeastern University, Boston, Massachusetts, USA

[b]Broad Institute of MIT and Harvard, CISID, Cambridge, Massachusetts, USA

#To whom correspondence should be addressed (e.geisinger@northeastern.edu)

Abstract

Phage have gained renewed interest as an adjunctive treatment for life-threatening infections with the resistant nosocomial pathogen *Acinetobacter baumannii*. Our understanding of how *A. baumannii* defends against phage remains limited, although this information could lead to improved antimicrobial therapies. To address this problem, we identified genome-wide determinants of phage susceptibility in *A. baumannii* using Tn-seq. These studies focused on the lytic phage Loki, which targets *Acinetobacter* by unknown mechanisms. We identified 41 candidate loci that increase susceptibility to Loki when disrupted, and 10 that decrease susceptibility. Combined with spontaneous resistance mapping, our results support the model that Loki uses the K3 capsule as an essential receptor, and that capsule modulation provides *A. baumannii* with strategies to control vulnerability to phage. A key center of this control is transcriptional regulation of capsule synthesis and phage virulence by the global regulator BfmRS. Mutations hyperactivating BfmRS simultaneously increase capsule levels, Loki replication, and host killing, while BfmRS-inactivating mutations have the opposite effect, reducing capsule and blocking Loki infection. We identified novel BfmRS-activating mutations, including knockouts of a T2 RNase protein and the disulfide formation enzyme DsbA, that hypersensitize bacteria to phage challenge. We further found that mutation of a glycosyltransferase known to alter capsule structure and bacterial virulence can also cause complete phage resistance. Finally, additional factors including lipooligosaccharide and Lon protease act independently of capsule modulation to interfere with Loki infection. This work demonstrates that regulatory and structural modulation of capsule, known to alter *A. baumannii* virulence, is also a major determinant of susceptibility to phage.

Author Summary

Antibiotic-resistant infections with *Acinetobacter baumannii* are a major problem in critical care units and have increased in frequency during the COVID-19 pandemic. The virulence of these infections depends on a polysaccharide capsule surrounding the bacterium. Phage, or viruses that kill bacteria, represent a promising alternative therapy against highly antibiotic-resistant *A. baumannii* infections, and *A. baumannii*-specific phage often target the capsule. Here, we use high-throughput genetics to analyze how *A. baumannii* defends against phage and identify ways to potentiate their killing activity. We found that stressing the bacteria in ways that cause augmented production of capsule also causes hyper-susceptibility to phage. By contrast, turning off the stress response, or mutating the capsule structure, causes complete phage resistance. Altering another surface structure, lipooligosaccharide, or an intracellular protease also enhances phage attack. Modulating the amounts or makeup of capsular polysaccharide is known to influence virulence in *A. baumannii*. This work thus uncovers a connection between phage pressure and the evolution of virulence in *A. baumannii*, and it identifies control mechanisms that may be leveraged for improving future phage-based antimicrobial therapies.

49 **Introduction**

50 The antibiotic-resistant, Gram-negative pathogen *Acinetobacter baumannii* is notorious
51 for causing recalcitrant diseases in healthcare settings including sepsis and ventilator-associated
52 pneumonia [1, 2]. Rates of *A. baumannii* infections resistant to last-line antibiotic treatments
53 have increased during the COVID-19 pandemic [3, 4], and pan-resistant isolates have emerged
54 [5, 6]. Therapy with lytic phages (viruses that infect and kill bacterial hosts) has gained renewed
55 attention as an additional line of attack against infections with pathogens such as *A. baumannii*
56 that are refractory to standard antibiotics. Phages have the benefit of having high host specificity,
57 allowing selective targeting of pathogens without broad damage to the microbiome.
58 Administration of anti-*A. baumannii* lytic phages in animal infection models has been efficacious
59 in conferring protection from disease [4, 7-12]. Moreover, recent successes in the clinic have
60 shown the promise of phage therapy as an adjunct to antibiotics for treating severe, progressive
61 multidrug-resistant *A. baumannii* infections in critically ill patients [13-15]. Phage may also
62 contribute to measures to block transmission of the pathogen in hospital environments [16].

63 Despite its potential, a drawback to phage therapy is the inevitable emergence of bacteria
64 resistant to phage attack [17]. In the case of *A. baumannii*, this drawback may be mitigated by
65 tradeoffs associated with phage resistance, such as lowered *in vivo* fitness/virulence, enhanced
66 antibiotic sensitivity, or both [12, 17-19]. These costs likely emerge due to the *A. baumannii*
67 capsule frequently serving as a requisite receptor for initiating phage infection [20-23].

68 Capsular polysaccharide is one of the most important virulence factors of *A. baumannii*
69 [24-26]. Acapsular escape mutants isolated after phage treatment in animal models show
70 dramatic attenuation similar to that documented for engineered capsule-null strains [12, 17, 18].
71 Although almost all *A. baumannii* patient isolates produce a capsule, the sugar compositions and

72 structures of the capsular polysaccharide have diversified greatly across strains [27, 28]. These
73 differences are in large part based on substitution of multiple genes within the highly variable K
74 locus, which determines subunit sugar synthesis, polymerization, and export of the capsular
75 polysaccharide [29, 30]. In some cases, structural changes can also manifest from variation in a
76 single gene in the K locus [26, 31]. Different capsule structures may influence the interface with
77 the host innate immune system, resulting in differences in how the capsule promotes
78 pathogenicity [26, 32-34]. In addition to interstrain structural variation, *A. baumannii* varies the
79 amount of capsule produced through regulatory networks. These capsule control networks
80 include those that sense and respond to antimicrobial stress [35, 36] or that stochastically switch
81 bacteria between two distinct phenotypic states [37-39], and each may contribute to how bacteria
82 adjust to changing host or environmental conditions. The degree to which modulation of capsule
83 levels affects susceptibility to phage attack is not known. Similarly, whether low-cost mutations
84 modifying (rather than eliminating) capsule can provide avenues to phage resistance is also
85 unclear. More broadly, functional characterization of *A. baumannii* determinants that facilitate or
86 impede phage infection is largely lacking. Knowledge of these features could lead to strategies
87 for improving the efficacy of anti-*A. baumannii* phage therapy and could enhance our
88 understanding of the physiology and resilience of the organism.

89 Here, we use a functional genomic approach to investigate determinants of *A. baumannii*-
90 phage interactions. We use Loki (vB_AbaS_Loki), a lytic phage of the *Siphoviridae* family that
91 was isolated from activated sludge using *A. baumannii* ATCC 17978 [40]. Analysis of the Loki
92 dsDNA genome has shown that it contains gene modules for virion morphogenesis, DNA
93 replication, and lysis, as well as an uncharacterized MazG-family protein of unknown function
94 [40]. The phage displays a narrow host range, infecting only 17978 among a panel of 40 diverse

95 isolates, suggesting the use of a strain-specific receptor of unknown identity [40]. A component
96 of the lipooligosaccharide (LOS) was suggested as the receptor, based on lack of Loki adsorption
97 to an *lpxA* mutant [40]. In the present study, we have identified the primary Loki host receptor as
98 the K3 capsule, and revealed pathways associated with capsule modulation that dramatically
99 alter bacterial sensitivity to phage attack. This work has implications for phage therapy against *A.*
100 *baumannii* and for understanding alteration of virulence in the pathogen.
101

102 **Results**

103 **High-throughput identification of phage susceptibility determinants in *A. baumannii*.**

104 Loki infection of *A. baumannii* 17978 results in small, turbid plaques on solid medium
105 and partial growth inhibition in liquid culture when using an initial multiplicity of infection
106 (MOI) of 1 or 10 (Fig 1A) [40]. These features show that Loki has low virulence with 17978. We
107 hypothesized that host mechanisms exist determining this outcome. To test this prediction and
108 investigate genome-wide bacterial determinants of phage susceptibility, we used Tn-seq, taking
109 advantage of our established strategies for identifying genetic determinants of antibiotic
110 susceptibility in 17978 [41, 42]. Ten independent *Mariner* insertion pools each having about
111 20,000 individual insertions [43] (~100,000 separate insertion sites in total) were grown for ~8
112 doublings in parallel in broth containing Loki at different initial MOIs (1 to 1.5, or 10 to 15), or
113 no phage (uninfected control). DNA was extracted from samples before (t_1) and after (t_2) the
114 outgrowth of each pool. Massively parallel sequencing was used to measure the frequency of
115 every transposon mutant in the population at each time point and calculate relative fitness (W)
116 [41, 42] (see Materials and Methods). We then aggregated all the mutant fitness values (across
117 all pools) associated with each gene to determine average, gene-level fitness scores (S1 Dataset).

118 Genes were identified that had decreased or increased Tn-seq fitness during phage challenge
119 compared to control, based on established criteria [fitness value derived from n ≥ 3 independent
120 insertion mutants, fitness difference ≥ 10%, and false-discovery rate (FDR) ≤ 0.05 [41, 42]] (see
121 Materials and Methods). These genes and their products are referred to as candidate phage
122 susceptibility determinants, and those associated with decreased fitness upon phage challenge
123 when mutated as candidate phage hypersusceptibility determinants.
124 Challenge with Loki at the lower MOI (1 to 1.5) resulted in 14 candidate phage
125 hypersusceptibility determinants (Fig 1B and S1 Dataset). The hits comprised numerous proteins
126 involved in biosynthesis and control of the bacterial cell envelope. These included *bfmS*, the
127 receptor of the BfmRS two-component system (TCS), which regulates capsule production,
128 virulence, and resistance in response to signals that are yet to be defined [35, 36, 44]; LOS core
129 oligosaccharide biosynthesis genes (*gtrOC2*, *gtrOC3*, *pda1*, *gtrOC4*, and *lpsB*) [29, 41]; and the
130 *dsbA* dithiol oxidase [45] critical for forming protein disulfide bonds in the Gram-negative
131 periplasm [46] (S1 Data Set). Additional hits were ACX60_RS02390 (referred to hereafter as
132 *rnaA*), encoding a predicted periplasmic RNase T2 homolog; the *lon* protease; and the *dksA*
133 transcription factor known to affect lytic phage infection in *E. coli* [47, 48].
134 Challenge with Loki at higher MOI (10 to 15) had two effects on the set of candidate
135 susceptibility determinants identified. First, the number of phage hypersusceptibility
136 determinants increased to 39 (Fig 1B and S1 Dataset). These hits included almost all (13/14)
137 those identified using MOI 1-1.5, as well as additional enzymes belonging to the above
138 functional categories (e.g., disulfide bond formation, *dsbC*, *dsbD*; LOS synthesis, *gtrOC8*; and
139 the protease *clpA*) and to new functional categories (e.g., the DNA adenine methyltransferase,
140 *aamA* [49]). Second, challenge with higher Loki MOI enabled detection of hits that had

141 increased fitness (i.e., decreased susceptibility) compared to controls (Fig 1B and S1 Dataset).
142 The strongest of these (showing greatest fitness increase and lowest q value) was *gne1*, which is
143 a K locus gene required for generating precursors for capsule biosynthesis [29]. Loss of Gne1
144 completely prevents capsule production [50]. Mutations in an additional K locus gene, *gtr9*,
145 which are also linked to capsule loss [19], also caused increased fitness during Loki challenge
146 (S1 Dataset). The other hits were extrinsic to the K locus, but several had annotations related to
147 polysaccharide production. The Tn-seq screen thus reveals a variety of candidate factors that
148 increase or decrease *A. baumannii* vulnerability to phage attack.
149

150 **Targeted deletion and complementation analyses validate the phage hypersusceptibility**
151 **phenotypes predicted by Tn-seq.**

152 We confirmed the Tn-seq results using individual mutant strains, focusing first on
153 candidate phage susceptibility determinants from different functional categories showing lower
154 Tn-seq fitness with Loki challenge (Fig 2A). Strains carrying in-frame deletions of *rnaA*, *dsbA*,
155 *gtrOC3*/*4*, and *lon* were constructed (Materials and Methods). To enable *trans* complementation
156 analysis, plasmids harboring an IPTG-inducible WT allele, or a control plasmid lacking the gene,
157 were introduced into the respective mutant strains (S1 Table). In the case of *bfmS*, in lieu of
158 complementation analysis we took advantage of multiple different mutants we previously
159 isolated in the *bfmRS* locus. This includes two *bfmS* mutants—a deletion with *aacC1*
160 replacement (referred to as Δ*bfmS*), and the frame-shift G467Dfs*19 [35] (referred to as
161 *bfmS**)—as well as additional mutants affecting *bfmR* as will be explained in a subsequent
162 section. Susceptibility to Loki was assessed by liquid challenge and plaque formation assays
163 (Materials and Methods). During liquid phage challenge, the *rnaA*, *dsbA*, and *bfmS* mutants all

164 showed complete block of growth immediately after exposure to Loki, unlike the WT, which
165 showed only partial growth inhibition after about 5 hours (Fig 2B and C). Different kinetics were
166 seen with Loki challenge of the other mutants. With the Δ*gtrOC3* and Δ*gtrOC4* mutants exposed
167 to phage, bacteria grew for an initial ~2.5 hours before collapse (Fig 2B). With Δ*lon*, by contrast,
168 Loki inhibited bacterial growth until ~4 hours, at which point rapid growth resumed (Fig 2B).
169 Reintroduction of the respective WT genes reversed the Loki hypersusceptibility phenotypes of
170 *rnaA, dsbA*, *gtrOC3*, *gtrOC4*, and *lon* mutants. In some cases, leaky expression without IPTG
171 was sufficient for partial (*dsbA*, *gtrOC4*) or full (*gtrOC3, lon*) complementation (Fig 2B).
172 Addition of IPTG at 0.1 mM allowed reversal of the Loki hypersusceptibility phenotype of all
173 strains, although a partial growth delay defect remained with the *rnaA* reintroduction strain
174 exposed to phage (Fig 2B). Raising the level of *rnaA* induction with 1 mM IPTG completely
175 eliminated this defect and had the added effect of rendering the strain even less susceptible to
176 Loki than the WT control (S1A Fig).
177 Results from plaque formation assays mirrored the findings from the liquid challenge
178 experiments. In contrast to the small, turbid plaques caused by Loki with control bacteria, the
179 same phage caused large, clear plaques with each candidate hypersusceptibility mutant (Fig 2D
180 and E). Plaques appeared to be larger with *rnaA, dsbA*, and *bfmS* mutants compared to *gtrOC3*
181 and *gtrOC4*, echoing the susceptibility differences seen with Loki challenge in broth (Fig 2,
182 compare D, E to B, C). Expressing the respective genes *in trans* with 1 mM IPTG reversed the
183 enhanced plaque phenotypes in all cases (Fig 2D). In particular, *rnaA* overexpression greatly
184 lowered the plaque formation efficiency of Δ*rnaA* beyond the level of the WT control, similar to
185 its effect during liquid challenge (Fig 2D and S1A Fig, compare Δ*rnaA*/*rnaA* to the WT control).

186 We note that the gene directly upstream of *rnaA*, ACX60_RS02385 (*slt* [36]), was also
187 identified as a candidate susceptibility determinant associated with modestly decreased fitness
188 during Loki challenge (S1 Dataset). Exposure of an in-frame Δ*slt* mutant to Loki recapitulated
189 the modest hypersusceptibility defect (S2A, B Fig). Analysis of the *slt* Tn-seq mutant fitness
190 values revealed a potentially biased distribution, with insertions causing major Loki
191 hypersusceptibility defects having an apparent bias toward the 3' end of the locus that is
192 proximal to *rnaA* (Fig 2A). The Δ*slt* mutant also showed slightly reduced levels of *rnaA*
193 expression (S2C Fig). Since phage susceptibility appears sensitive to *rnaA* expression level (Fig
194 2B, D, E), we cannot rule out a polar effect on *rnaA* in the altered phage susceptibility of the *slt*
195 mutant, and this mutant was not pursued further. These results underscore that candidate Loki
196 hypersusceptibility loci identified through Tn-seq show the predicted susceptibility phenotypes
197 when analyzed independently using engineered mutant strains.
198
199 **Analysis of Loki resistance mutations reveals capsular polysaccharide as phage receptor.**
200 Given the identification of capsule production genes as sites of mutations that increase fitness
201 during phage challenge (S1 Dataset), we tested the hypothesis that the capsule is essential to the
202 infective cycle of Loki by serving as a host receptor. To this end, we examined the Tn-seq data
203 associated with the entire K locus of 17978 (KL3) and additional genes involved in capsule
204 production. Gene-level Tn-seq fitness scores were available for 9 out of 20 KL3 genes. The other
205 11 were represented by too few transposon mutants, as observed previously, likely due to their
206 essential involvement in late steps of capsule biosynthesis that may cause dead-end intermediates
207 when blocked [43]. For most of the 9 permissive KL3 genes, transposon disruption led to higher
208 fitness during Loki exposure relative to untreated control (with 5 having non-FDR $P < 0.05$; Fig

209 3A). Disruption of *wzi*, an additional permissive gene outside the K locus that encodes the lectin
210 required for efficient surface binding of capsular polysaccharide [51], also increased Tn-seq
211 fitness during Loki challenge compared to control, albeit without passing statistical cut-offs (P =
212 0.15). Since a subset of the glycan building blocks encoded by the K locus are used for protein
213 glycosylation by PglL [52], we also examined the *pglL* Tn-seq phenotypes. In contrast to the
214 capsule synthesis genes, transposon insertions in *pglL* showed slightly decreased fitness during
215 Loki challenge (Fig 3A). These findings indicate that lesions leading to capsule deficiency are
216 associated with enhanced fitness in the face of Loki challenge, while the opposite is true for *pglL*
217 mutations, which are known to eliminate protein O-glycans but preserve capsule [52].
218 Building on these observations, we determined the requirement of capsule for Loki
219 infection by examining (1) targeted capsule mutants, (2) additional clinical isolates of diverse
220 capsule types, and (3) spontaneous phage-resistant mutants. First, we analyzed deletions in
221 17978 of two critical capsule synthesis genes: *itrA*, the initiating transferase required for use of
222 phosphosugars in both capsule synthesis and protein O-glycosylation and *wzc*, essential to
223 assembly and export of high-molecular weight capsular polysaccharide [29, 35, 52]. Δ*itrA* causes
224 loss of both capsule and protein O-glycans, while Δ*wzc* blocks capsule specifically. We note that
225 unlike *itrA*, *wzc* is essential in 17978 [35, 43]. Δ*wzc* could be analyzed, however, by the parallel
226 use of EGA106-27, which is a viable 17978 Δ*wzc* isolate harboring extragenic compensatory
227 mutations, and EGA260, its isogenic *wzc*-repaired derivative obtained by marker rescue [35]. As
228 predicted by Tn-seq, deletion of *itrA* led to increased growth during Loki challenge in liquid
229 (S3A Fig) and completely blocked plaque formation (Fig 3B). Reintroduction of *itrA* reversed
230 this defect, with the resulting susceptibility to Loki dependent on the level of *itrA* induction (Fig
231 3B; S3A Fig). Loki was also completely unable to form plaques on EGA106-27 (Wzc^-), but

232 readily infected EGA260 (Wzc^{+}) (Fig. 3B). The plaques on EGA260 were larger and clearer than
233 that seen with the WT control, presumably a consequence of the compensatory mutations
234 rendering it hypersensitive to phage. The Loki non-susceptibility of ItrA-deficient (capsule^{-}
235 /protein O-glycan^{-}) and Wzc-deficient (capsule^{-}/protein O-glycan^{+}) strains, and the
236 hypersusceptibility detected with *pglL* transposon mutants (capsule^{+}/protein O-glycan^{-}), points to
237 capsular polysaccharide as essential for phage infection.

238 Second, we found that the K3 capsule type correlates with the ability of diverse clinical
239 isolates to be targeted by Loki. To determine Loki host range we used strains 17978, 17961 and
240 19606, which all have KL3; BAA-1790 [53], which has KL22 (identical to KL3 but with one
241 extra gene; Fig. 3D); and AB5075, which has the unrelated KL25 cluster. Note that both KL3
242 and KL22 biosynthetic gene clusters yield the same capsular polysaccharide, type K3 [27, 54],
243 while the K25 capsule generated from KL25 has a completely different structure [55]. Loki
244 formed plaques on all four K3 strains, but not the K25 strain (Fig. 3C). Ability to infect was
245 independent of the type of LOS outer core biosynthesis locus (OCL) in the host strains (Fig. 3C).
246 These results are consistent with the K3 capsule, and not LOS outer core, providing a specific
247 host receptor for Loki infection.

248 Third, analysis of spontaneous Loki-resistant mutants supported the model that capsule
249 provides an essential, specific receptor for Loki. Three independent 17978 mutants forming
250 colonies within zones of confluent lysis were isolated and their genomes were sequenced
251 (Materials and Methods). Each strain had a single, slipped-strand mispairing mutation within
252 homopolymeric sites in the K locus (Fig 3D). Two were identical mutations (440A$_{9\rightarrow8}$) in *gtr6*,
253 encoding a glycosyltransferase that adds a single sugar side-chain to the capsule repeat unit [26]
254 (S2 Table), and the third was in the *wzx* polysaccharide flippase (377T$_{9\rightarrow10}$) [29]. Each mutation

255 caused a frameshift and premature translation termination. While deficiency of Wzx is expected
256 to result in complete capsule loss, Gtr6 deficiency is known to preserve capsule but cause an
257 altered structure lacking the side chain sugar [26]. Intriguingly, *gtr6* deletion was recently shown
258 to amplify 17978 virulence during bloodstream infection in mice, and a naturally occurring *gtr6*
259 mutation (1008::IS*Aba13*) was found to drive hypervirulence in another K3 isolate, HUMC1
260 [26]. We confirmed that 17978 *gtr6*440A$_{9\rightarrow8}$ resists Loki plaque formation, a phenotype reversed
261 by reintroduction of WT *gtr6* (Fig 3E) and recapitulated by an in-frame *gtr6* deletion (S3B Fig).
262 Consistent with previous findings that loss of Gtr6 alters capsule structure but not amount [26],
263 *gtr6*440A$_{9\rightarrow8}$ and Δ*gtr6* caused no change to overall capsule levels (S4A Fig). Search of public
264 databases revealed that the 440A$_{9\rightarrow8}$ allele is present in a variety of KL3 and KL22 *A. baumannii*
265 clinical isolates (S2 Table and ref. [56]), consistent with this site as a mutational hotspot in *gtr6*.
266 We also examined *gtr6* within two strains harboring KL22 from our sequenced *A. baumannii*
267 clinical isolate collection, EGA10 and EGA65. We found that both strains have a novel IS*Aba13*
268 insertion near 440A (425::IS*Aba*13), resembling the situation with HUMC1 [26]. EGA10 and
269 EGA65 were both Loki-resistant, but introducing WT *gtr6* from 17978 had the dramatic effect of
270 conferring Loki susceptibility with efficient plaque formation (Fig 3E). These results further
271 support the K3 capsule as a specific Loki receptor, and suggest that *gtr6* is a hub for mutations
272 linking phage evasion to the evolution of *A. baumannii* virulence.
273 Finally, we examined the effect of *itrA*, *gtr6*, and *wzc* mutations on phage adsorption
274 (Materials and Methods). Each mutation resulted in loss of Loki attachment, as indicated by high
275 fractions of phage remaining in suspension after mixture with bacteria (Fig 4A). Together these
276 results support the conclusion that Loki uses the K3 capsule as an essential receptor.
277

278 **BfmRS activity controls phage susceptibility.**

279 Loki-hypersensitizing *bfmS* mutations lead to capsule hyperproduction by increasing
280 transcription of capsule biosynthesis genes [35], likely through enhanced activity of the cognate
281 transcription factor BfmR [44]. Controlling BfmR activity and capsule production could thereby
282 also allow control of *A. baumannii* susceptibility to phage. We tested this model by analyzing
283 mutations in *bfmR*, which cause phenotypes opposite those of *bfmS* mutants including decreased
284 capsule production [35]. *bfmR* mutants are thus predicted to be less susceptible to capsule-
285 targeting phage. In the Tn-seq screen, *bfmR* transposon mutants indeed had increased fitness
286 during Loki challenge relative to controls, particularly at the higher MOIs, in stark contrast to the
287 dramatic hypersusceptibility of *bfmS* mutants (Fig 5A). To confirm the altered phage
288 susceptibility phenotype associated with *bfmR*, we used a knockout of the entire TCS (Δ*bfmRS*),
289 which phenocopies a single *bfmR* deletion [35, 36, 44] and shows reduced capsule levels
290 compared to WT and the hyper-encapsulated *bfmS** mutant (Fig 5B). As predicted by Tn-seq,
291 Δ*bfmRS* is impervious to Loki in both liquid challenge and plaque assays (Fig 5C, D). Given this
292 non-susceptibility and the epistatic relationship of *bfmR* to *bfmS*, we predicted that spontaneous
293 phage-resistance mutations in the hypersusceptible *bfmS** strain would map to *bfmR*. To test this
294 prediction, mutants of *bfmS** forming colonies within zones of lysis by Loki were isolated and
295 analyzed by whole-genome sequencing. In two mutants, the resistance mutations were indeed in
296 *bfmR*, causing amino acid substitutions G100D and T85I. Each mutation completely prevented
297 Loki infection in either liquid (Fig 5C) or plaque (Fig 5D) assays, despite the hypersusceptibility
298 of the parent strain. G100 and T85 are highly conserved residues near the BfmR dimerization
299 interface and the predicted site of phosphorylation, respectively, based on the published crystal
300 structure [57, 58]. T85 also aligns with the "switch" residue of *E. coli* CheY (T87), in which a

301 similar mutation to isoleucine blocks phosphorylation-induced conformational changes and
302 activation [59]. G100D and T85I are thus predicted to inactivate BfmR. Consistent with
303 inactivation, both substitutions greatly reduced the phosphorylated (predicted active [44])
304 fraction of the protein (BfmR~P, Fig 5E) as well as total BfmR amounts (S5A Fig), as analyzed
305 in phosphate affinity shift gels (Materials and Methods). The BfmR substitutions also reduced
306 capsule synthesis to levels seen with Δ*bfmRS* (Fig 5B). We note that in other Loki-escape
307 derivatives of *bfmS**, *gtr6* was again a site of mutations, including two independent $440A_{9\rightarrow8}$
308 mutations and another, novel slipped-strand mispairing mutation within a different poly-A tract
309 ($384A_{8\rightarrow7}$) (Fig 3D, S2 Table).
310 The opposing effects on capsule and Loki susceptibility of *bfmR* (low capsule, low
311 infectivity) and *bfmS* (high capsule, high infectivity) mutants are consistent with regulation of the
312 capsule receptor contributing to the differential sensitivity to Loki in each strain. In agreement
313 with this model, compared to WT, Loki showed reduced adsorption to Δ*bfmRS* and dramatically
314 increased adsorption to *bfmS** (slow vs rapid decline in the fraction of free phage, respectively,
315 Fig 4B). The increased adsorption and infectivity of Loki conferred by *bfmS* mutation depended
316 on the K3 capsule, based on two lines of evidence. First, deleting *itrA* or *gtr6* in 17978 *bfmS*
317 mutants blocked Loki adsorption (S6A Fig) and killing (S6B Fig). Second, *bfmS* mutation
318 greatly enhanced Loki plaque formation in 19606 (K3), but had no effect on Loki susceptibility
319 in AB5075 (K25) (S6C Fig). These data thereby further support the notion that the BfmRS-
320 dependent boost in Loki susceptibility depends on capsule.
321
322 **Defects in RnaA and DsbA control capsule and phage susceptibility through BfmRS**

323 We reasoned that additional lesions uncovered in our genome-wide screen may owe their
324 altered Loki susceptibility to modulation of the capsule receptor. We found that knockouts of
325 *rnaA* and *dsbA* in 17978, which hypersensitize the bacteria to Loki, also each increased capsule
326 production (by ~50%, Fig 6A) and phage surface adsorption (Fig 4B), similar to the
327 enhancements caused by *bfmS* mutation. As expected, augmented capsule production was
328 reversed by expressing each WT allele in trans (S1B Fig).
329 To determine if the link between capsule biosynthesis, phage susceptibility, and *rnaA* and
330 *dsbA* applies to a different K3 strain, we also deleted the genes in BAA-1790. Similar to their
331 effects in 17978, each deletion caused BAA-1790 to hyperproduce capsule (Fig. 6C) and
332 increase susceptibility to Loki (S7A Fig). Because the BAA-1790 WT parent showed complete
333 resistance to Loki in the liquid challenge assay, we also tested a mutant derivative of Loki
334 (Loki*, Materials and Methods) with increased virulence against WT strains (S7B Fig and Fig.
335 6D, WT). Δ*rnaA* and Δ*dsbA* each caused BAA-1790 to be completely inhibited by Loki* under
336 conditions in which the WT showed minimal inhibition (Fig. 6D). RnaA and DsbA lesions thus
337 amplify capsule and phage susceptibility in both a laboratory strain carrying KL3 as well as a
338 more recent, carbapenem-resistant clinical isolate carrying KL22, suggesting that the proteins act
339 through a conserved envelope modulation pathway.
340 Given the highly similar capsule and phage susceptibility phenotypes shared by *rnaA*,
341 *dsbA*, and *bfmS* mutants, and the ability of the BfmRS regulatory system activity to control these
342 phenotypes, we considered the possibility that *rnaA* and *dsbA* mutations act through BfmRS. We
343 thus defined the epistatic relationship of the TCS to *rnaA* and *dsbA* in 17978. We found that
344 combining Δ*rnaA* or Δ*dsbA* with Δ*bfmRS* led to low capsule levels (Fig 6A) and complete
345 resistance to phage attack in both liquid challenge (Fig 6B) and plaque formation assays (S1C

346 Fig), mirroring the Δ*bfmRS* single mutant phenotypes. In addition, we examined how *rnaA*
347 overexpression interacts with the TCS, taking advantage of the above observation that
348 overexpression of *rnaA*, but not *dsbA*, not only complements the corresponding deletion but also
349 lowers capsule and Loki susceptibility below WT levels (Fig 2D; S1A,B Fig). We predicted that
350 these decreases would depend on BfmRS. We found that overexpressing *rnaA* in trans in WT led
351 to lower levels of capsule compared to uninduced control (Fig 6E), and completely prevented
352 Loki plaque formation (Fig 6F). Both of these effects were blocked when *rnaA* induction
353 occurred in a *bfmS** strain harboring the inactive version of the BfmS receptor (Fig 6E, F). In
354 contrast to the results with *rnaA* and as predicted from Fig 2D, overexpressing *dsbA* in WT did
355 not inhibit plaque formation (S1D Fig). Together, these results are consistent with the model that
356 RnaA and DsbA defects act through BfmRS to modulate capsule and Loki infectivity, with the
357 TCS sensing relative levels of RnaA and presence/absence of DsbA function.

358 Several additional lines of evidence support the model that BfmRS responds to RnaA and
359 DsbA defects. First, Δ*rnaA* and Δ*dsbA* mutants increased the transcription of capsule
360 biosynthesis genes (*wza* and *gnaA*, Fig 7A) and the activity of a BfmRS-dependent promoter
361 fused to GFP (18040p-GFP, Fig 7B), mirroring the effects of *bfmS* mutation on the same
362 phenotypes [36]. Similar increases were not seen with a BfmRS-independent reporter construct
363 (*adc*p-GFP [36], Fig 7B), or with 18040p-GFP when Δ*rnaA* or Δ*dsbA* were combined with
364 Δ*bfmRS* (Fig 7C). The reporter results indicate that transcriptional enhancement by RnaA and
365 DsbA deficiency is specific and dependent on BfmRS. Second, Δ*rnaA* and Δ*dsbA* each increased
366 the fraction of BfmR~P by approximately 3-fold (Fig 7D) and appeared to increase total BfmR
367 levels as well (S5B Fig), similar to the effects of *bfmS* deletion. Third, analysis of previous
368 genome-wide fitness datasets [41] revealed that *rnaA*, *dsbA,* and *bfmS* mutants have highly

369 correlated antibiotic susceptibility profiles (phenotypic signatures), which are likely to reflect
370 functional connectivity between the genes (Fig 7E and S1E Fig, $r = 0.58\text{-}0.67$, $p < 0.0005$). The
371 *bfmS*, *rnaA*, and *dsbA* signatures also positively correlated with those of other *A. baumannii* Dsb
372 system homologs (DsbB, DsbD, and at least one of 3 DsbC paralogs, ACX60_RS16880),
373 suggesting that disulfide bond formation in general is linked to the functions of BfmS and RnaA.
374 Mutations in *dsbB*, *dsbD* and the same *dsbC* paralog (RS16880) also showed decreased Tn-seq
375 fitness during Loki challenge, albeit not to the degree seen with *dsbA* (Fig 7F). Fourth, our
376 previous RNA-seq data [36] showed that expression of several *dsb* genes as well as *rnaA* is
377 under the control of BfmRS, with *bfmR* and *bfmS* mutants having differential effects on their
378 transcription (S1F Fig). Finally, while the Δ*rnaA*, Δ*dsbA*, and Δ*bfmRS* individual mutants and the
379 Δ*rnaA* Δ*bfmRS* combined mutant do not show substantially impaired growth at 37°C, we found
380 that combining Δ*dsbA* and Δ*bfmRS* results in a synthetic growth defect (Fig 7G). This result
381 implies that BfmRS protects *A. baumannii* from DsbA deficiency and the consequent defects in
382 periplasmic protein disulfide bonds, consistent with a toxicity-stress response relationship.
383 Sequence analysis of RnaA, an RNase-domain protein, sheds light on its connection to
384 DsbA and BfmRS. RnaA contains a signal peptide as well as eight cysteine residues (S8 Fig).
385 These features potentially place RnaA in the periplasm where internal disulfide bonds could be
386 formed by DsbA, as occurs with its *E. coli* ortholog, RNase I [60]. Unlike RNase I, however,
387 RnaA and its close orthologs within *Acinetobacter* and *Psychrobacter* completely lack the
388 catalytic histidines and other key residues in its two conserved active sites (CAS) critical for
389 RNase activity (S8 Fig) [61], as previously noted with the *A. baumannii* RnaA sequence [62].
390 These findings suggest that RnaA may be a pseudoenzyme, whose levels and/or folding may
391 influence BfmS signaling and phage susceptibility.

392

393 **Factors influencing phage infection independent of capsule modulation**

394 While modulation of capsule is a major feature of altered Loki susceptibility, we found
395 that other hypersusceptibility determinants—including *gtrOC3*, *gtrOC4*, and *lon*—affect
396 vulnerability to Loki independently of regulating the capsule receptor. Deletions of these genes
397 resulted in growth defects during phage challenge in liquid medium that were characterized by
398 different kinetics compared to those of the hypo-encapsulated *rnaA*, *dsbA*, and *bfmS* mutants (Fig
399 2B, C), consistent with an alternate mechanism underlying their susceptibility defects.

400 Deletions of *gtrOC3* and *gtrOC4*, which encode predicted LOS outer core
401 glycosyltransferases [29], resulted in the expected enrichment of truncated forms of LOS without
402 lowering the overall amount of LOS produced (Fig 8A). The deletions also showed no change to
403 the levels or size distribution of capsular polysaccharide compared to the WT control (S4B Fig).
404 Despite having WT levels of the capsule receptor, the Δ*gtrOC3* and Δ*gtrOC4* mutants both
405 showed similar enhancements to Loki adsorption, particularly at the later 10 and 20 minute time
406 points (Fig 4B). As noted above, mutating other LOS outer core synthesis genes also decreased
407 fitness during Loki challenge compared to controls, albeit to a lesser extent than *gtrOC3* and
408 *gtrOC4* (Fig 8B, S1 Dataset). This suggests that a range of outer core defects can affect Loki
409 susceptibility. By combining additional mutations with Δ*gtrOC3*, we found that its enhanced
410 Loki attachment and susceptibility phenotypes still depended on initial binding to capsule. A
411 Δ*gtrOC3* Δ*itrA* double mutant showed complete lack of Loki adsorption (S6D Fig), and
412 Δ*gtrOC3* Δ*itrA* and Δ*gtrOC3* Δ*gtr6* double mutants showed full phage resistance in solid and
413 liquid media (Fig 8C, D). The full-length LOS outer core thus functions to inhibit the ability of

414 Loki to efficiently adhere to and infect *A. baumannii*, likely after the initial requisite interaction
415 with capsule.
416 Deleting *lon* caused no significant change to capsular polysaccharide levels (S4C Fig),
417 consistent with previous observations [63], and had no effect on LOS quantity or banding pattern
418 (S9C Fig). As predicted from the lack of major changes to the key surface components, Loki
419 adsorption was not significantly enhanced with the Δ*lon* mutant vs WT; rather, adsorption
420 appeared lowered at the early 5-min time point compared to WT (Fig 4C). Lon protease may
421 thus be affecting susceptibility to Loki by influencing a lytic cycle step occurring after surface
422 interactions.
423 We considered the possibility that the altered Loki susceptibility of mutants showing
424 altered capsule production could also involve alterations to LOS. We therefore examined LOS
425 from the *bfmRS*, *bfmS*, *rnaA* and *dsbA* deletion mutants. LOS from Δ*bfmRS*, Δ*rnaA* and Δ*dsbA*
426 showed no differences in banding pattern or total levels compared to LOS from WT (S9A,B
427 Fig). While overall amounts of LOS from Δ*bfmS* were not significantly altered, we observed the
428 appearance of a single, novel band migrating slightly faster than the full-length LOS (S9A Fig,
429 arrowhead). This band may represent an LOS intermediate, although it is slower migrating and
430 much less abundant than the major intermediate band enriched in Δ*gtrOC3* and Δ*gtrOC4*
431 mutants. Thus, while altered capsule receptor abundance is a key feature of the enhanced Loki
432 susceptibility of BfmRS-hyperactive bacteria, a contribution of altered LOS to the dramatic
433 hypersusceptibility of *bfmS* mutants cannot yet be ruled out.
434
435 **Enhanced phage multiplication caused by BfmRS hyperactivity and Lon deficiency.**

436 To examine how phage hypersusceptibility loci affect Loki intracellular replication, we
437 performed one-step phage growth analysis (Materials and Methods). The results of these
438 experiments are shown in Table 1 and S10 Fig. Infection of WT bacteria resulted in a burst size
439 of ~20 plaque-forming units (PFU) per infective center and an eclipse period of ~40 minutes.
440 Compared to this control, *bfmS** led to a dramatic amplification in phage replication, increasing
441 burst size >10-fold and shortening the eclipse by half. BfmRS-hyperactive Δ*rnaA* and Δ*dsbA*
442 mutations had similar effects, increasing the burst 3-5-fold and halving the eclipse period. These
443 results indicate that the BfmRS pathway shapes phage susceptibility not only by affecting
444 adsorption but also by controlling intracellular phage replication. Δ*lon* also increased Loki burst
445 size (by 7-fold) and shortened the eclipse phase by ~10min, consistent with the above idea that
446 Lon primarily influences post-adsorption phage growth. By contrast, Δ*gtrOC3* showed no
447 change in the magnitude of phage replication, indicating that LOS outer core synthesis mainly
448 affects phage adsorption.
449

450 **Table 1. Results from one-step growth experiments.**
451

Host strain[a]	eclipse period (min)[b]	Burst size: mean ± SEM (PFU)	Burst size: adjusted p-value[c]	n
WT	40	20.6 ± 1.2		12
bfmS*	20	225.9 ± 17.9	<0.0001	4
Δ***rnaA***	20	61.8 ± 9.9	0.0069	4
Δ***dsbA***	20	94.9 ± 6.0	<0.0001	4
Δ***gtrOC3***	30	27.3 ± 1.8	0.9843	4
Δ***lon***	30	141.2 ± 19.7	<0.0001	4

452
453 a. *A. baumannii* 17978 background
454 b. mode value from experiments using 10-minute sampling intervals
455 c. from one-way ANOVA with Šídák's multiple comparisons test (comparing each mutant vs WT)
456

457 **Discussion**

458 Bacteriophage show promise as an alternative therapy against drug-resistant bacteria, but
459 how vulnerability to phage attack can be controlled is poorly understood. In this work we have
460 defined the genome-wide mechanisms of *A. baumannii* susceptibility to killing by phage Loki.
461 Our results support a model in which this susceptibility is determined by numerous major factors
462 affecting the efficiency of phage adsorption and post-adsorption replication (Fig. 9A). We found
463 that capsule type K3 provides the primary Loki receptor. LOS outer core glycans antagonize
464 adsorption likely by impeding access to a secondary binding site, which could be membrane-
465 proximal residues of the capsule or of the LOS molecule (e.g., the conserved LOS inner core).
466 Phage adsorption as well as intracellular phage replication are controlled in dual fashion by the
467 BfmRS regulatory system (Fig. 9A). Activating the TCS augments capsule production and phage
468 growth, while deactivating the TCS lowers capsule and confers complete resistance (Fig. 9B, C).
469 Lon is another defense factor that specifically limits phage multiplication (Fig. 9A, C). How
470 BfmRS and Lon control phage growth dynamics intracellularly remains to be defined. Of note,
471 the hypersusceptibility seen with *A. baumannii* mutants showing capsule overproduction or Lon
472 deficiency stand in contrast to the situation in *E. coli,* in which these features are associated with
473 broad phage resistance [64, 65]. Finally, alteration of capsule structure through naturally
474 occurring glycosyltransferase mutations provides an additional pathway to phage resistance
475 through loss of adsorption (Fig. 9B). The *gtr6* locus appears to be a hotspot for such mutations,
476 related to strand slippage and insertion sequence elements, that could potentially facilitate
477 variation of capsule structure within bacterial populations [66, 67].

478 *A. baumannii* phages frequently target specific host capsules [26, 35-38]. That capsule
479 structural modulation mediates phage escape has implications for strategies to control the

480 evolution of *A. baumannii* phage resistance and virulence. Mutations in *gtr6*, which determines
481 the addition of N-acetyl-β-D-glucosamine branches on the K3 capsule backbone [26], are known
482 to amplify virulence [26]. Our findings thus suggest that phage, in the environment or during
483 therapy, may impose selective pressures facilitating the evolution of altered capsules with the
484 potential collateral effect of increasing pathogenicity. Notably, a repeat region within another
485 predicted side-chain glycosyltransferase, *gtr76*, was a site of mutations in phage-resistant K116
486 *A. baumannii* isolated from a patient receiving phage therapy [23], although effects on capsule
487 structure were not determined. Mutational capsule loss is an additional, well-described phage
488 escape mechanism (Fig. 9B) usually associated with lowered *in vivo* fitness and other trade-offs,
489 making this form of resistance an appealing target of sequential or combination therapies
490 exploiting the trade-offs [18, 68]. Our data, and potentially those of [23], argue that capsule-loss
491 mutations should not be considered a universally predictable path of *A. baumannii* phage
492 resistance and that capsule-altered mutants maintaining (and possibly enhancing) virulence
493 should also be considered. This may be particularly relevant when targeting specific capsules
494 such as K3. Combining phages to target both $Gtr6^+$ and $Gtr6^-$ [56] capsules may allow treatment
495 of K3 *A. baumannii* infections while blocking the rise of undesired mutants. In sum, these
496 observations support the notion that prior research into resistance mechanisms can enhance the
497 predictability of bacterial evolution during phage exposure and may allow improvements to the
498 therapeutic uses of phage [18, 23, 68].

499 Controlling the abundance of capsule is also tightly connected to modulation of
500 virulence, and we show here that this control has the additional effect of modulating phage
501 susceptibility, with implications for developing phage-drug synergies [68-70] and for
502 understanding variable capsule production in the pathogen. *A. baumannii* regulates capsule

503 synthesis through multiple mechanisms, including the BfmRS stress response and stochastic
504 phenotypic switching systems, and the regulatory states associated with higher capsule
505 production show increased virulence [35-38]. We show that BfmRS hyperactivity is an Achilles'
506 heel that can be exploited by capsule-targeting phages, allowing them to bind, multiply, and kill
507 with enhanced efficiency. It is possible that antimicrobials that increase capsule [35] could
508 similarly potentiate phage activity, while the opposite may be seen with antagonists of
509 BfmRS/capsule production. Chemical inhibitors of DsbA [46, 71], which would activate BfmRS
510 and capsule synthesis while impairing envelope proteins generally, represent an attractive
511 candidate strategy for small molecule potentiation of phage attack. Regarding the basis of
512 variable capsule production, our results raise the possibility that environmental phage are among
513 the putative selective pressures that enrich low-capsule (translucent) variants arising from
514 stochastic phenotype switching [37].

515 By examining determinants of Loki susceptibility acting through BfmRS, this work
516 provides new leads into the signals detected by the virulence-resistance regulator, which have
517 remained poorly defined. We reveal that changes in DsbA and RnaA generate signals sensed by
518 the TCS, leading to transcriptional control of capsule and phage infectivity. The finding that
519 lesions affecting periplasmic disulfide bonds generate a stress-response has a parallel in the *E.*
520 *coli* Cpx system [72]. *dsbA* mutants activate Cpx [73], which in turn regulates *dsbA* in a feedback
521 loop [74, 75]. In *A. baumannii*, expression of *dsb* and oxidative stress response genes is
522 modulated by BfmRS [36, 44]. These findings reinforce the view that BfmRS has a subset of
523 activities analogous to those of Cpx [24]. As noted above, several observations connect DsbA to
524 RnaA. A major substrate of DsbA in *E. coli* is the RnaA ortholog RNase I, a non-essential,
525 periplasmic, broad-substrate endonuclease [60]. RNase I and RnaA both have eight cysteines,

526 but RnaA is likely non-catalytic, and its levels serve as a BfmRS signal. A possible interpretation
527 is that *Acinetobacter* has coopted its RNase T2 family protein to function as a sensor of envelope
528 disulfide bond defects and/or oxidative damage. It is worth noting that a sensor of disulfide bond
529 defects has been reported in *E. coli*, NlpE, which transmits signals to Cpx [73]. *A. baumannii* has
530 an NlpE ortholog but it lacks the domain implicated in disulfide sensing [76]. This suggests that
531 the pathogen uses a distinct strategy to monitor periplasmic disulfides, with consequences for
532 vulnerability to phage. Future work will focus on investigating this strategy and defining the
533 connections between RnaA, oxidative folding stress, and BfmS in protecting and altering the *A.*
534 *baumannii* cell envelope.

535 In addition to capsule control pathways, our data with LOS outer core glycosyltransferase
536 mutants support an important role for outer core glycans in defending against Loki attack. It is
537 possible that the outer core hinders phage binding to a more internal secondary receptor. Another
538 possibility is that Loki's preferred secondary receptor is a truncated form of LOS, whose levels
539 increase in *gtrOC* mutants, increasing adsorption efficiency. Previous work showed that
540 mutation of *lpxA*, which completely prevents LOS production, is also reported to block Loki
541 adsorption [40]. This could be explained by the loss of a putative secondary binding site as noted
542 above, and/or by loss of capsule when LOS synthesis is completely arrested [77]. Examination of
543 additional LOS variants should assist in defining the precise mechanisms by which LOS
544 participates in phage infection and defense.

545 In conclusion, we have analyzed the genome-wide determinants of susceptibility to
546 bacteriophage Loki in *A. baumannii* and identified multiple mechanisms that modulate phage
547 infectivity, including several linked to altered bacterial virulence. Our results expose a
548 vulnerability in a pathogenic strategy of *A. baumannii*, capsule hyperproduction, that allows

549 enhanced killing by the capsule-specific phage. Additional work is needed to define the novel
550 stress sensing mechanisms that impact on phage virulence, how cytoplasmic factors control
551 intracellular viral multiplication, and how the susceptibility factors identified here affect
552 infection by additional families of *Acinetobacter* phages. Future studies focusing on
553 manipulation of phage hypersusceptibility pathways in *A. baumannii* may facilitate the
554 development of improved phage-based combination therapies targeting the pathogen.
555

556 **Materials and Methods**

557 **Strains and growth conditions.** Bacterial strains used in this work are described in S1 Table. *A.*
558 *baumannii* strains were derivatives of ATCC 17978 unless otherwise noted. Bacteria were
559 cultured in Lysogeny Broth (10 g/L tryptone, 5 g/L yeast extract, 10 g/L NaCl) (LB). Cultures
560 were incubated at 37°C in all cases except phage infection experiments, which used 30°C unless
561 otherwise indicated. LB + 5mM $CaCl_2$ was used as culture medium in all phage infection
562 experiments. Liquid cultures were aerated with orbital shaking or with rotation via roller drum,
563 with growth monitored by measuring optical density (OD) as absorbance at 600nm (A_{600}). LB
564 agar (1.5% w/v) plates were supplemented with antibiotics as needed (tetracycline [Tc] at 10
565 µg/ml; carbenicillin [Cb] at 50-100 µg/ml, kanamycin [Km] at 10-20 µg/ml, gentamicin [Gm] at
566 10 µg/ml) or sucrose (10% w/v) (Sigma). Isopropyl β-D-thiogalactoside (IPTG) (Sigma) was
567 added to cultures at 0.1-1 mM for induction of P(IPTG)-controlled constructs. Super optimal
568 broth with catabolite repression (SOC) was used in Tn-seq library preparation. Bacteriophage
569 Loki (vB_AbaS_Loki)[40] was a gift from Dann Turner. A derivative of Loki (Loki*) was
570 isolated by purifying phage from a clear plaque forming within a zone of turbid 17978 lysis.
571

572 **Molecular cloning and strain construction.** Oligonucleotide primers and plasmids used in this
573 study are listed in Table S1. Most sequences were PCR-amplified from the *A. baumannii* 17978
574 genome and cloned in pUC18 before subcloning to destination plasmids. Clones were verified by
575 DNA sequencing (Genewiz/Azenta). Gene deletions were constructed in-frame by allele
576 exchange with cloned ~1kb homology arms using conditionally replicating vectors pSR47S or
577 pJB4648 and sucrose counterselection as described [35]. Deletion mutants were verified by
578 verified by colony PCR. An AB5075 *bfmS*::Tn mutant was obtained from the Manoil lab Three-
579 Allele Transposon Mutant Library and verified by screening for TcR and whole-genome
580 sequencing. For complementation and overexpression experiments, sequences were subcloned
581 downstream of the *lacI*^{q}-T5*lac*P module [P(IPTG)] on plasmid pYDE152. Plasmids were
582 delivered into *A. baumannii* by electroporation.
583
584 **Phage-challenge Tn-seq.** Stocks of *A. baumannii* ATCC 17978 *Mariner* transposon mutants
585 constructed previously [43] were thawed, revived for 1 hour in LB, and then back diluted to
586 OD=0.005 (~2.5×10^6 CFU/ml) in LB with 5mM $CaCl_2$ containing Loki at MOI 1 (or 1.5), at
587 MOI of 10 (or 15), or no phage (uninfected control). Cultures were incubated at 37°C until each
588 reached OD ~1 (about 8 doublings). This took approximately 2 hours for control cultures, with
589 additional time, usually 15-20 minutes, given to the phage treatment arms as needed to reach the
590 target OD. 10 banks of ~20,000 mutants per bank were analyzed independently. Genomic DNA
591 (gDNA) was extracted (Qiagen DNeasy) from samples before and after the 8 doublings,
592 quantified by a SYBR green I (Invitrogen) microtiter assay, and tagmented (Illumina Nextera).
593 Transposon-adjacent DNA was then amplified to form Illumina libraries as described [41, 42].
594 Libraries were size-selected (Pippin HT, 275bp-600bp) and sequenced (single-end 50 bp) using

595 primer mar512 [41] on a HiSeq 2500 with high output V4 chemistry at the Tufts University
596 Genomics Core Facility (TUCF-Genomics).
597 Sequencing read data were processed, mapped to the 17978 chromosome
598 (NZ_CP012004) and pAB3 (NZ_CP012005), and used to calculate individual transposon mutant
599 fitness (*W*) based on mutant vs population-wide expansion in each condition using our published
600 pipeline and formula [41]. Fitness values were standardized across conditions by normalizing to
601 the average value of insertions in neutral sites (pseudogenes and endogenous transposon-related
602 genes) within the genome predicted to have no effects on growth. Gene-level average fitness was
603 calculated by averaging the fitness values of all individual mutants in a given condition across all
604 pools having a transposon in the first 90% of the gene. Difference in gene-level fitness between
605 phage-challenge and control conditions was deemed significant if it had a magnitude >10%,
606 derived from $n \geq 3$ individual mutants, and had q-value <0.05 in unpaired, two-tailed t test with
607 FDR controlled by the Benjamini, Krieger, and Yekutieli two-stage step-up method (Prism 8).
608 Fitness values at genomic loci were visualized with Integrative Genomics Viewer [78] after
609 aggregation across all transposon mutant libraries via the SingleFitness script [79].
610
611 **Phage susceptibility analysis.**
612 *i. Liquid challenge.* Bacterial cultures were diluted to OD=0.003 in LB + 5mM $CaCl_2$ and
613 combined with phage at an MOI=1 or with no phage (uninfected control). Bacterial growth was
614 monitored during incubation at 30°C in microtiter plates in an Epoch 2 or Synergy H1M plate
615 reader (Biotek).
616 *ii. Plaque formation assay.* Bacterial cultures were diluted to OD=1 in 100µl of LB, combined
617 with 5ml of top agar (LB with 5mM $CaCl_2$ and 0.4% w/v agar), and poured onto LB agar plates.

618 10-fold serial dilutions of phage in Saline-magnesium diluent plus gelatin (SMG) buffer (50mM
619 Tris-HCl, PH=7.5, 100mM NaCl, 8mM MgSO4, 0.01% (W/V) gelatin) [80] were spotted onto
620 the top agar, and plates were incubated at 30°C for 16 hours. Plaques were imaged with white
621 light transillumination using a Chemidoc MP (Bio-Rad).
622 *iii. Phage adsorption.* Host bacteria were cultured in LB + 5mM $CaCl_2$ at 30°C to OD=0.1. Loki
623 was added at MOI=0.1 followed by incubation at 30°C. At regular time intervals, 100µl were
624 sampled and mixed with 100µl SMG buffer saturated with chloroform. After centrifugation
625 (8000 x g, 5 minutes), unadsorbed phage within supernatants was enumerated by plaque
626 formation assay. The fraction of free phage was calculated as the number of PFU at each time
627 point divided by the total input PFU.
628 iv. *One-step phage growth*. Host bacteria were cultured as in *iii* to OD=0.1. Loki was added at
629 MOI=0.05 in 1 ml volume and allowed to adsorb for 5 minutes. Mixtures were centrifuged (4000
630 x g, 2 minutes) and supernatants containing unadsorbed phage were removed and used to
631 determine unadsorbed PFUs. Pellets were resuspended in sterile LB + 5mM $CaCl_2$ and incubated
632 at 30°C. 100µl samples were taken immediately (T0) and at 10-minute intervals over 90 minutes.
633 Samples were combined with 50µl chloroform and used to determine post-adsorption PFUs.
634 Burst size was calculated by dividing the average PFU from samples at the plateau of phage
635 growth by the infected cell number. Infected cell number was calculated by subtracting the
636 unadsorbed PFU from the total input PFU. Data were combined from two independent
637 experiments, each experiment performed in biological duplicate and with a WT host control arm.
638
639 **Whole-genome sequencing of spontaneous phage-nonsusceptibility mutants and clinical**
640 **isolates**. Bacterial mutants (derived from *A. baumannii* 17978 WT, *bfmS**, or Δ*bfmS*) forming

641 colonies within areas of Loki lysis/plaquing were purified on LB agar. gDNA was extracted and
642 quantified as above. Illumina libraries were prepared by a modified Nextera method [36] and
643 sequenced (single-end 100) on a HiSeq 2500 at TUCF-Genomics. Variants were identified from
644 sequencing reads by Breseq as described [81, 82]. Mutations were verified by PCR amplification
645 and Sanger sequencing (Genewiz/Azenta). EGA10 and EGA65 genomes were sequenced and
646 hybrid assembled at SeqCenter using sequencing data from Illumina (NextSeq 2000, 2x151bp)
647 and Oxford Nanopore platforms. The genome assemblies were used for species confirmation and
648 MLST strain type determination [83]. K and outer core locus types were determined from
649 genome sequence data using bioinformatics tools [84, 85].
650
651 **Capsular polysaccharide analysis.** Capsular polysaccharide was extracted from processed cell
652 lysates and analyzed by alcian blue following described protocols [35]. Samples were collected
653 from early post-exponential phase cultures (OD 2-3) and centrifuged. Cell pellets were
654 resuspended with lysis buffer [60mM Tris, pH 8; 10mM $MgCl_2$; 50µM $CaCl_2$; 20µl/ml DNase
655 (NEB) and RNase cocktail (Amersham); and 3mg/ml lysozyme (Sigma)] and incubated at 37°C
656 for 1 hour. Samples were further processed by 3 liquid nitrogen/37°C freeze-thaw cycles and
657 stepwise treatments with additional DNase and RNase (37°C, 30 minutes), 0.5% SDS (37°C, 30
658 minutes), and Proteinase K (NEB, 60°C, 1 hour). Samples were combined with SDS-PAGE
659 loading buffer, boiled for 5 minutes, and separated on 4-20% Bio-Rad TGX Tris-glycine gels.
660 Capsule was stained with Alcian blue (Sigma), imaged via white light transillumination
661 (ChemiDoc MP), and quantified using Image Lab (Bio-Rad).
662

663 **LOS analysis.** LOS was analyzed via Tricine gel electrophoresis of cell lysates as described
664 [41]. Log phase bacteria were washed with PBS, resuspended with Novex tricine SDS sample
665 buffer (Invitrogen, 50µl 1X buffer per 0.5 OD units of bacteria), and boiled for 15 minutes.
666 Samples were separated on Novex 16% tricine gels (Invitrogen) and stained with Pro-Q Emerald
667 300 (Invitrogen). Gels were imaged using UV transillumination (ChemiDoc MP). Total protein
668 detected with subsequent Coomassie Brilliant Blue staining was used for sample normalization.
669 Relative values were calculated by dividing each normalized LOS value by the total normalized
670 LOS levels in WT [41].
671
672 **Gene expression analysis.** For RT-qPCR, RNA was extracted from log phase bacteria (Qiagen
673 RNeasy), DNase treated (Turbo DNA-free kit, Invitrogen), and reverse transcribed (Superscript
674 II Reverse Transcriptase, Invitrogen). cDNA served as template in qPCR with gene-specific
675 primers (S1 Table) and SYBR Green Master Mix (Applied Biosystems) using a StepOnePlus
676 system according to the manufacturer's instructions. The amplification efficiency for each pair
677 was tested by standard curves using serial diluted cDNA, and found to be > 97% in each case.
678 Fold change in gene expression was calculated by using the $2^{-\Delta\Delta Ct}$ method with *rpoC* as
679 endogenous control [36]. qPCR was performed in technical duplicate from biological triplicate
680 samples. Samples lacking reverse transcriptase were used to confirm absence of signal from
681 residual gDNA. For fluorescence reporter analysis, bacteria were harvested from OD=1 cultures,
682 resuspended in PBS, and transferred to a black, clear bottom microplate (Corning 3631).
683 Fluorescence intensity (excitation at 480 nm/emission at 520 nm) and A_{600} were measured with a
684 Synergy H1M (Biotek). Density-normalized fluorescence units were calculated as fluorescence
685 intensity/A_{600}.

686

687 **Analysis of BfmR phosphorylation.** Phosphate affinity electrophoresis was performed
688 following published protocols [86]. 1 OD of mid-log phase bacteria were resuspended in 55µl of
689 BugBuster reagent with 0.1% (v/v) Lysonase (Novagen). Lysis was assisted by repeated
690 pipetting. 18µl of 4X SDS sample buffer (200mM Tris-HCl pH 6.8, 8% SDS, 0.4%
691 Bromophenol blue, 40% Glycerol) was added, and lysates were electrophoresed in Phos-Tag gels
692 [12% acrylamide, 50µM Phos-tag acrylamide (Wako Chemicals), and 100 µM $MnCl_2$] at 30mA.
693 After electrophoresis, gels were incubated for 10 minutes in 1X transfer buffer (50mM Tris,
694 380mM Glycine, 0.1% SDS, 20% Methanol) with 1mM EDTA to remove manganese, followed
695 by additional 10 minutes in transfer buffer without EDTA. Proteins were transferred to PVDF
696 membranes (100V, 1hr). Total protein was detected in the blots with SYPRO Ruby blot stain
697 (Invitrogen) using the manufacturer's instructions and a GelDoc EZ (Bio-Rad). Blots were
698 incubated in blocking buffer (5% Milk in TBS-T, 1 hour, room temperature) and probed with
699 rabbit anti-BfmR antiserum (1:30,000 or 1:90,000 in blocking buffer, overnight at 4C) and goat
700 anti-rabbit-HRP secondary antibody (Invitrogen, 1:5,000 in blocking buffer, 1 hour at room
701 temperature). Blots were washed 3x10 minutes in TBS-T before and after incubation with
702 secondary antibody, and washed 10min in TBS before developing. Signals were detected with
703 Western Lightning Plus-ECL (Perkin Elmer) and a ChemiDoc MP, and quantified using Image
704 Lab. Rabbit anti-BfmR antiserum was generated by immunizing a rabbit with purified
705 recombinant BfmR according to standard protocols (Pocono Rabbit Farm and Laboratory).

706

707 **Phenotypic signature analysis.** Tn-seq phenotypic signatures belonging to *bfmS*, *rnaA*, and *dsb*
708 paralogs in *A. baumannii* were extracted from previous genome-wide datasets [41]. Hierarchical

709 clustering was performed by the average linkage method using Qlucore Omics Explorer (3.7).

710 Pearson correlation analysis was performed using Prism 9.

711

712 **Acknowledgements**

713 We thank Dann Turner for the gift of phage Loki and Colin Manoil for the AB5075 *bfmS*::Tn

714 strain. We are grateful to Isabella Bailey, Sarah Hudson, and Wenwen Huo for their technical

715 assistance, and members of the Geisinger lab for helpful discussions.

716 **References**
717
718 1. Doi Y, Murray GL, Peleg AY. *Acinetobacter baumannii*: evolution of antimicrobial
719 resistance-treatment options. Semin Respir Crit Care Med. 2015;36(1):85-98. doi: 10.1055/s-
720 0034-1398388. PMID: 25643273.
721 2. Weiner-Lastinger LM, Abner S, Edwards JR, Kallen AJ, Karlsson M, Magill SS, et al.
722 Antimicrobial-resistant pathogens associated with adult healthcare-associated infections:
723 Summary of data reported to the National Healthcare Safety Network, 2015-2017. Infect Control
724 Hosp Epidemiol. 2019:1-18. Epub 2019/11/27. doi: 10.1017/ice.2019.296. PMID: 31767041.
725 3. CDC. COVID-19: U.S. Impact on Antimicrobial Resistance, Special Report 2022.
726 Atlanta, GA: U.S. Department of Health and Human Services, CDC, 2022.
727 4. Rangel K, Chagas TPG, De-Simone SG. *Acinetobacter baumannii* Infections in Times of
728 COVID-19 Pandemic. Pathogens. 2021;10(8). Epub 2021/08/29. doi:
729 10.3390/pathogens10081006. PMID: 34451470.
730 5. Nowak J, Zander E, Stefanik D, Higgins PG, Roca I, Vila J, et al. High incidence of
731 pandrug-resistant *Acinetobacter baumannii* isolates collected from patients with ventilator-
732 associated pneumonia in Greece, Italy and Spain as part of the MagicBullet clinical trial. J
733 Antimicrob Chemother. 2017;72(12):3277-82. Epub 2017/09/30. doi: 10.1093/jac/dkx322.
734 PMID: 28961773.
735 6. Qureshi ZA, Hittle LE, O'Hara JA, Rivera JI, Syed A, Shields RK, et al. Colistin-resistant
736 *Acinetobacter baumannii*: beyond carbapenem resistance. Clin Infect Dis. 2015;60(9):1295-303.
737 Epub 2015/01/30. doi: 10.1093/cid/civ048. PMID: 25632010.
738 7. Ghaznavi-Rad E, Komijani M, Moradabadi A, Rezaei M, Shaykh-Baygloo N. Isolation of
739 a lytic bacteriophage against extensively drug-resistant *Acinetobacter baumannii* infections and
740 its dramatic effect in rat model of burn infection. J Clin Lab Anal. 2022;36(7):e24497. Epub
741 2022/06/17. doi: 10.1002/jcla.24497. PMID: 35708005.
742 8. Hua Y, Luo T, Yang Y, Dong D, Wang R, Wang Y, et al. Phage Therapy as a Promising
743 New Treatment for Lung Infection Caused by Carbapenem-Resistant *Acinetobacter baumannii*
744 in Mice. Front Microbiol. 2017;8:2659. Epub 2018/01/30. doi: 10.3389/fmicb.2017.02659.
745 PMID: 29375524.
746 9. Kusradze I, Karumidze N, Rigvava S, Dvalidze T, Katsitadze M, Amiranashvili I, et al.
747 Characterization and Testing the Efficiency of *Acinetobacter baumannii* Phage vB-GEC_Ab-M-
748 G7 as an Antibacterial Agent. Front Microbiol. 2016;7:1590. Epub 2016/10/21. doi:
749 10.3389/fmicb.2016.01590. PMID: 27757110.
750 10. Wang Y, Mi Z, Niu W, An X, Yuan X, Liu H, et al. Intranasal treatment with
751 bacteriophage rescues mice from *Acinetobacter baumannii*-mediated pneumonia. Future
752 Microbiol. 2016;11:631-41. Epub 2016/03/02. doi: 10.2217/fmb.16.11. PMID: 26925593.
753 11. Wu M, Hu K, Xie Y, Liu Y, Mu D, Guo H, et al. A Novel Phage PD-6A3, and Its
754 Endolysin Ply6A3, With Extended Lytic Activity Against *Acinetobacter baumannii*. Front
755 Microbiol. 2018;9:3302. Epub 2019/01/29. doi: 10.3389/fmicb.2018.03302. PMID: 30687281.
756 12. Regeimbal JM, Jacobs AC, Corey BW, Henry MS, Thompson MG, Pavlicek RL, et al.
757 Personalized Therapeutic Cocktail of Wild Environmental Phages Rescues Mice from
758 *Acinetobacter baumannii* Wound Infections. Antimicrob Agents Chemother. 2016;60(10):5806-
759 16. Epub 2016/07/20. doi: 10.1128/AAC.02877-15. PMID: 27431214.
760 13. Nir-Paz R, Gelman D, Khouri A, Sisson BM, Fackler J, Alkalay-Oren S, et al. Successful
761 Treatment of Antibiotic-resistant, Poly-microbial Bone Infection With Bacteriophages and

762 Antibiotics Combination. Clin Infect Dis. 2019;69(11):2015-8. Epub 2019/03/15. doi:
763 10.1093/cid/ciz222. PMID: 30869755.
764 14. Rao S, Betancourt-Garcia M, Kare-Opaneye YO, Swierczewski BE, Bennett JW, Horne
765 B, et al. Critically Ill Patient with Multidrug-Resistant *Acinetobacter baumannii* Respiratory
766 Infection Successfully Treated with Intravenous and Nebulized Bacteriophage Therapy.
767 Antimicrob Agents Chemother. 2022;66(1):e0082421. Epub 2021/10/19. doi:
768 10.1128/AAC.00824-21. PMID: 34662188.
769 15. Schooley RT, Biswas B, Gill JJ, Hernandez-Morales A, Lancaster J, Lessor L, et al.
770 Development and Use of Personalized Bacteriophage-Based Therapeutic Cocktails To Treat a
771 Patient with a Disseminated Resistant *Acinetobacter baumannii* Infection. Antimicrob Agents
772 Chemother. 2017;61(10). Epub 2017/08/16. doi: 10.1128/AAC.00954-17. PMID: 28807909.
773 16. Chen LK, Chang JC, Chu HT, Chen YT, Jiang HL, Wang LS, et al. Preoptimized phage
774 cocktail for use in aerosols against nosocomial transmission of carbapenem-resistant
775 *Acinetobacter baumannii*: A 3-year prospective intervention study. Ecotoxicol Environ Saf.
776 2022;236:113476. Epub 2022/04/04. doi: 10.1016/j.ecoenv.2022.113476. PMID: 35367880.
777 17. Gordillo Altamirano FL, Barr JJ. Phage Therapy in the Postantibiotic Era. Clin Microbiol
778 Rev. 2019;32(2). Epub 2019/01/18. doi: 10.1128/CMR.00066-18. PMID: 30651225.
779 18. Gordillo Altamirano FL, Kostoulias X, Subedi D, Korneev D, Peleg AY, Barr JJ. Phage-
780 antibiotic combination is a superior treatment against *Acinetobacter baumannii* in a preclinical
781 study. EBioMedicine. 2022;80:104045. Epub 2022/05/11. doi: 10.1016/j.ebiom.2022.104045.
782 PMID: 35537278.
783 19. Wang X, Loh B, Gordillo Altamirano F, Yu Y, Hua X, Leptihn S. Colistin-phage
784 combinations decrease antibiotic resistance in *Acinetobacter baumannii* via changes in envelope
785 architecture. Emerg Microbes Infect. 2021;10(1):2205-19. Epub 2021/11/06. doi:
786 10.1080/22221751.2021.2002671. PMID: 34736365.
787 20. Abdelkader K, Gutierrez D, Latka A, Boeckaerts D, Drulis-Kawa Z, Criel B, et al. The
788 Specific Capsule Depolymerase of Phage PMK34 Sensitizes *Acinetobacter baumannii* to Serum
789 Killing. Antibiotics (Basel). 2022;11(5). Epub 2022/05/29. doi: 10.3390/antibiotics11050677.
790 PMID: 35625321.
791 21. Gordillo Altamirano F, Forsyth JH, Patwa R, Kostoulias X, Trim M, Subedi D, et al.
792 Bacteriophage-resistant *Acinetobacter baumannii* are resensitized to antimicrobials. Nat
793 Microbiol. 2021;6(2):157-61. Epub 2021/01/13. doi: 10.1038/s41564-020-00830-7. PMID:
794 33432151.
795 22. Popova AV, Shneider MM, Arbatsky NP, Kasimova AA, Senchenkova SN, Shashkov
796 AS, et al. Specific Interaction of Novel Friunavirus Phages Encoding Tailspike Depolymerases
797 with Corresponding *Acinetobacter baumannii* Capsular Types. J Virol. 2020. Epub 2020/12/04.
798 doi: 10.1128/JVI.01714-20. PMID: 33268523.
799 23. Liu M, Hernandez-Morales A, Clark J, Le T, Biswas B, Bishop-Lilly KA, et al.
800 Comparative genomics of *Acinetobacter baumannii* and therapeutic bacteriophages from a
801 patient undergoing phage therapy. Nat Commun. 2022;13(1):3776. Epub 2022/07/01. doi:
802 10.1038/s41467-022-31455-5. PMID: 35773283.
803 24. Geisinger E, Huo W, Hernandez-Bird J, Isberg RR. *Acinetobacter baumannii*: Envelope
804 Determinants That Control Drug Resistance, Virulence, and Surface Variability. Annu Rev
805 Microbiol. 2019;73:481-506. Epub 2019/06/18. doi: 10.1146/annurev-micro-020518-115714.
806 PMID: 31206345.

807 25. Oliveira H, Mendes A, Fraga AG, Ferreira A, Pimenta AI, Mil-Homens D, et al. K2
808 Capsule Depolymerase Is Highly Stable, Is Refractory to Resistance, and Protects Larvae and
809 Mice from *Acinetobacter baumannii* Sepsis. Appl Environ Microbiol. 2019;85(17). Epub
810 2019/06/23. doi: 10.1128/AEM.00934-19. PMID: 31227554.
811 26. Talyansky Y, Nielsen TB, Yan J, Carlino-Macdonald U, Di Venanzio G, Chakravorty S,
812 et al. Capsule carbohydrate structure determines virulence in *Acinetobacter baumannii*. PLoS
813 Pathog. 2021;17(2):e1009291. Epub 2021/02/03. doi: 10.1371/journal.ppat.1009291. PMID:
814 33529209.
815 27. Giguere D. Surface polysaccharides from *Acinetobacter baumannii*: Structures and
816 syntheses. Carbohydr Res. 2015;418:29-43. Epub 2015/11/05. doi: 10.1016/j.carres.2015.10.001.
817 PMID: 26531136.
818 28. Koeleman JG, van der Bijl MW, Stoof J, Vandenbroucke-Grauls CM, Savelkoul PH.
819 Antibiotic resistance is a major risk factor for epidemic behavior of *Acinetobacter baumannii*.
820 Infect Control Hosp Epidemiol. 2001;22(5):284-8. Epub 2001/06/29. doi: ICHE6806 [pii]
821 10.1086/501901. PMID: 11428438.
822 29. Kenyon JJ, Hall RM. Variation in the complex carbohydrate biosynthesis loci of
823 *Acinetobacter baumannii* genomes. PLoS One. 2013;8(4):e62160. Epub 2013/04/25. doi:
824 10.1371/journal.pone.0062160. PMID: 23614028.
825 30. Kenyon JJ, Hall RM. Updated Analysis of the Surface Carbohydrate Gene Clusters in a
826 Diverse Panel of *Acinetobacter baumannii* Isolates. Antimicrob Agents Chemother.
827 2022;66(1):e0180721. Epub 2021/10/19. doi: 10.1128/AAC.01807-21. PMID: 34662195.
828 31. Shashkov AS, Kenyon JJ, Senchenkova SN, Shneider MM, Popova AV, Arbatsky NP, et
829 al. *Acinetobacter baumannii* K27 and K44 capsular polysaccharides have the same K unit but
830 different structures due to the presence of distinct wzy genes in otherwise closely related K gene
831 clusters. Glycobiology. 2016;26(5):501-8. Epub 2015/12/30. doi: 10.1093/glycob/cwv168.
832 PMID: 26711304.
833 32. Huang X, Li X, An H, Wang J, Ding M, Wang L, et al. Capsule type defines the
834 capability of *Klebsiella pneumoniae* in evading Kupffer cell capture in the liver. PLoS Pathog.
835 2022;18(8):e1010693. Epub 2022/08/02. doi: 10.1371/journal.ppat.1010693. PMID: 35914009.
836 33. Hathaway LJ, Grandgirard D, Valente LG, Tauber MG, Leib SL. *Streptococcus*
837 *pneumoniae* capsule determines disease severity in experimental pneumococcal meningitis. Open
838 Biol. 2016;6(3). Epub 2016/03/25. doi: 10.1098/rsob.150269. PMID: 27009189.
839 34. Melin M, Trzcinski K, Meri S, Kayhty H, Vakevainen M. The capsular serotype of
840 *Streptococcus pneumoniae* is more important than the genetic background for resistance to
841 complement. Infect Immun. 2010;78(12):5262-70. Epub 2010/09/22. doi: 10.1128/IAI.00740-10.
842 PMID: 20855513.
843 35. Geisinger E, Isberg RR. Antibiotic modulation of capsular exopolysaccharide and
844 virulence in *Acinetobacter baumannii*. PLoS Pathog. 2015;11(2):e1004691. Epub 2015/02/14.
845 doi: 10.1371/journal.ppat.1004691. PMID: 25679516.
846 36. Geisinger E, Mortman NJ, Vargas-Cuebas G, Tai AK, Isberg RR. A global regulatory
847 system links virulence and antibiotic resistance to envelope homeostasis in *Acinetobacter*
848 *baumannii*. PLoS Pathog. 2018;14(5):e1007030. Epub 2018/05/26. doi:
849 10.1371/journal.ppat.1007030. PMID: 29795704.
850 37. Chin CY, Tipton KA, Farokhyfar M, Burd EM, Weiss DS, Rather PN. A high-frequency
851 phenotypic switch links bacterial virulence and environmental survival in *Acinetobacter*

852 *baumannii*. Nat Microbiol. 2018;3(5):563-9. Epub 2018/04/26. doi: 10.1038/s41564-018-0151-5.
853 PMID: 29693659.
854 38. Tierney ARP, Chin CY, Weiss DS, Rather PN. A LysR-Type Transcriptional Regulator
855 Controls Multiple Phenotypes in *Acinetobacter baumannii*. Front Cell Infect Microbiol.
856 2021;11:778331. Epub 2021/11/23. doi: 10.3389/fcimb.2021.778331. PMID: 34805000.
857 39. Tipton KA, Chin CY, Farokhyfar M, Weiss DS, Rather PN. Role of Capsule in
858 Resistance to Disinfectants, Host Antimicrobials, and Desiccation in *Acinetobacter baumannii*.
859 Antimicrob Agents Chemother. 2018;62(12). Epub 2018/10/10. doi: 10.1128/AAC.01188-18.
860 PMID: 30297362.
861 40. Turner D, Wand ME, Briers Y, Lavigne R, Sutton JM, Reynolds DM. Characterisation
862 and genome sequence of the lytic *Acinetobacter baumannii* bacteriophage vB_AbaS_Loki. PLoS
863 One. 2017;12(2):e0172303. Epub 2017/02/17. doi: 10.1371/journal.pone.0172303. PMID:
864 28207864.
865 41. Geisinger E, Mortman NJ, Dai Y, Cokol M, Syal S, Farinha A, et al. Antibiotic
866 susceptibility signatures identify potential antimicrobial targets in the *Acinetobacter baumannii*
867 cell envelope. Nature Communications. 2020;11(1):4522. doi: 10.1038/s41467-020-18301-2.
868 42. Geisinger E, Vargas-Cuebas G, Mortman NJ, Syal S, Dai Y, Wainwright EL, et al. The
869 Landscape of Phenotypic and Transcriptional Responses to Ciprofloxacin in *Acinetobacter*
870 *baumannii*: Acquired Resistance Alleles Modulate Drug-Induced SOS Response and Prophage
871 Replication. MBio. 2019;10(3). Epub 2019/06/13. doi: 10.1128/mBio.01127-19. PMID:
872 31186328.
873 43. Bai J, Dai Y, Farinha A, Tang AY, Syal S, Vargas-Cuebas G, et al. Essential gene
874 analysis in *Acinetobacter baumannii* by high-density transposon mutagenesis and CRISPR
875 interference. J Bacteriol. 2021;203(12). Epub 2021/03/31. doi: 10.1128/JB.00565-20. PMID:
876 33782056.
877 44. Palethorpe S, Farrow JM, 3rd, Wells G, Milton ME, Actis LA, Cavanagh J, et al.
878 *Acinetobacter baumannii* Regulates Its Stress Responses via the BfmRS Two-Component
879 Regulatory System. J Bacteriol. 2022;204(2):e0049421. Epub 2021/12/07. doi:
880 10.1128/JB.00494-21. PMID: 34871031.
881 45. Premkumar L, Kurth F, Duprez W, Groftehauge MK, King GJ, Halili MA, et al.
882 Structure of the *Acinetobacter baumannii* dithiol oxidase DsbA bound to elongation factor EF-
883 Tu reveals a novel protein interaction site. J Biol Chem. 2014;289(29):19869-80. Epub
884 2014/05/27. doi: 10.1074/jbc.M114.571737. PMID: 24860094.
885 46. Landeta C, Boyd D, Beckwith J. Disulfide bond formation in prokaryotes. Nat Microbiol.
886 2018;3(3):270-80. Epub 2018/02/22. doi: 10.1038/s41564-017-0106-2. PMID: 29463925.
887 47. Cech GM, Kloska A, Krause K, Potrykus K, Cashel M, Szalewska-Palasz A. Virus-Host
888 Interaction Gets Curiouser and Curiouser. PART I: Phage P1vir Enhanced Development in an *E.*
889 *coli* DksA-Deficient Cell. Int J Mol Sci. 2021;22(11). Epub 2021/06/03. doi:
890 10.3390/ijms22115890. PMID: 34072628.
891 48. Patterson-West J, James TD, Fernandez-Coll L, Iben JR, Moon K, Knipling L, et al. The
892 *E. coli* Global Regulator DksA Reduces Transcription during T4 Infection. Viruses. 2018;10(6).
893 Epub 2018/06/09. doi: 10.3390/v10060308. PMID: 29882792.
894 49. Blaschke U, Suwono B, Zafari S, Ebersberger I, Skiebe E, Jeffries CM, et al.
895 Recombinant production of A1S_0222 from *Acinetobacter baumannii* ATCC 17978 and
896 confirmation of its DNA-(adenine N6)-methyltransferase activity. Protein Expr Purif.
897 2018;151:78-85. Epub 2018/06/18. doi: 10.1016/j.pep.2018.06.009. PMID: 29908915.

898 50. Harding CM, Haurat MF, Vinogradov E, Feldman MF. Distinct amino acid residues
899 confer one of three UDP-sugar substrate specificities in *Acinetobacter baumannii* PglC
900 phosphoglycosyltransferases. Glycobiology. 2018;28(7):522-33. Epub 2018/04/19. doi:
901 10.1093/glycob/cwy037. PMID: 29668902.
902 51. Tickner J, Hawas S, Totsika M, Kenyon JJ. The Wzi outer membrane protein mediates
903 assembly of a tight capsular polysaccharide layer on the *Acinetobacter baumannii* cell surface.
904 Sci Rep. 2021;11(1):21741. Epub 2021/11/07. doi: 10.1038/s41598-021-01206-5. PMID:
905 34741090.
906 52. Lees-Miller RG, Iwashkiw JA, Scott NE, Seper A, Vinogradov E, Schild S, et al. A
907 common pathway for O-linked protein-glycosylation and synthesis of capsule in *Acinetobacter*
908 *baumannii*. Mol Microbiol. 2013;89(5):816-30. Epub 2013/06/21. doi: 10.1111/mmi.12300.
909 PMID: 23782391.
910 53. Korotetskiy IS, Joubert M, Magabotha SM, Jumagaziyeva AB, Shilov SV, Suldina NA,
911 et al. Complete Genome Sequence of Collection Strain *Acinetobacter baumannii* ATCC BAA-
912 1790, Used as a Model To Study the Antibiotic Resistance Reversion Induced by Iodine-
913 Containing Complexes. Microbiol Resour Announc. 2020;9(3). Epub 20200116. doi:
914 10.1128/MRA.01467-19. PMID: 31948971.
915 54. Hamidian M, Blasco L, Tillman LN, To J, Tomas M, Myers GSA. Analysis of Complete
916 Genome Sequence of *Acinetobacter baumannii* Strain ATCC 19606 Reveals Novel Mobile
917 Genetic Elements and Novel Prophage. Microorganisms. 2020;8(12). Epub 2020/12/02. doi:
918 10.3390/microorganisms8121851. PMID: 33255319.
919 55. Senchenkova SN, Shashkov AS, Popova AV, Shneider MM, Arbatsky NP, Miroshnikov
920 KA, et al. Structure elucidation of the capsular polysaccharide of *Acinetobacter baumannii*
921 AB5075 having the KL25 capsule biosynthesis locus. Carbohydr Res. 2015;408:8-11. Epub
922 2015/03/31. doi: 10.1016/j.carres.2015.02.011. PMID: 25816997.
923 56. Timoshina OY, Kasimova AA, Shneider MM, Arbatsky NP, Shashkov AS, Shelenkov
924 AA, et al. Loss of a Branch Sugar in the *Acinetobacter baumannii* K3-Type Capsular
925 Polysaccharide Due To Frameshifts in the *gtr6* Glycosyltransferase Gene Leads To
926 Susceptibility To Phage APK37.1. Microbiol Spectr. 2023;11(1):e0363122. Epub 20230118. doi:
927 10.1128/spectrum.03631-22. PMID: 36651782.
928 57. Draughn GL, Milton ME, Feldmann EA, Bobay BG, Roth BM, Olson AL, et al. The
929 Structure of the Biofilm-controlling Response Regulator BfmR from *Acinetobacter baumannii*
930 Reveals Details of Its DNA-binding Mechanism. J Mol Biol. 2018;430(6):806-21. Epub
931 2018/02/14. doi: 10.1016/j.jmb.2018.02.002. PMID: 29438671.
932 58. Russo TA, Manohar A, Beanan JM, Olson R, MacDonald U, Graham J, et al. The
933 Response Regulator BfmR Is a Potential Drug Target for *Acinetobacter baumannii*. mSphere.
934 2016;1(3). doi: 10.1128/mSphere.00082-16. PMID: 27303741.
935 59. Ganguli S, Wang H, Matsumura P, Volz K. Uncoupled phosphorylation and activation in
936 bacterial chemotaxis. The 2.1-A structure of a threonine to isoleucine mutant at position 87 of
937 CheY. J Biol Chem. 1995;270(29):17386-93. Epub 1995/07/21. PMID: 7615544.
938 60. Messens J, Collet JF, Van Belle K, Brosens E, Loris R, Wyns L. The oxidase DsbA folds
939 a protein with a nonconsecutive disulfide. J Biol Chem. 2007;282(43):31302-7. Epub
940 2007/08/19. doi: 10.1074/jbc.M705236200. PMID: 17702751.
941 61. Deshpande RA, Shankar V. Ribonucleases from T2 family. Crit Rev Microbiol.
942 2002;28(2):79-122. Epub 2002/07/12. doi: 10.1080/1040-840291046704. PMID: 12109772.

943 62. Jacobs AC, Blanchard CE, Catherman SC, Dunman PM, Murata Y. An ribonuclease T2
944 family protein modulates *Acinetobacter baumannii* abiotic surface colonization. PLoS One.
945 2014;9(1):e85729. Epub 2014/02/04. doi: 10.1371/journal.pone.0085729. PMID: 24489668.
946 63. Ching C, Yang B, Onwubueke C, Lazinski D, Camilli A, Godoy VG. Lon Protease Has
947 Multifaceted Biological Functions in *Acinetobacter baumannii*. J Bacteriol. 2019;201(2). Epub
948 2018/10/24. doi: 10.1128/JB.00536-18. PMID: 30348832.
949 64. Kortright KE, Chan BK, Turner PE. High-throughput discovery of phage receptors using
950 transposon insertion sequencing of bacteria. Proc Natl Acad Sci U S A. 2020;117(31):18670-9.
951 Epub 2020/07/18. doi: 10.1073/pnas.2001888117. PMID: 32675236.
952 65. Kim MS, Kim YD, Hong SS, Park K, Ko KS, Myung H. Phage-encoded colanic acid-
953 degrading enzyme permits lytic phage infection of a capsule-forming resistant mutant
954 *Escherichia coli* strain. Appl Environ Microbiol. 2015;81(3):900-9. Epub 20141121. doi:
955 10.1128/AEM.02606-14. PMID: 25416767.
956 66. Henderson IR, Owen P, Nataro JP. Molecular switches--the ON and OFF of bacterial
957 phase variation. Mol Microbiol. 1999;33(5):919-32. doi: 10.1046/j.1365-2958.1999.01555.x.
958 PMID: 10476027.
959 67. Whiteway C, Valcek A, Philippe C, Strazisar M, De Pooter T, Mateus I, et al. Scarless
960 excision of an insertion sequence restores capsule production and virulence in *Acinetobacter*
961 *baumannii*. ISME J. 2022;16(5):1473-7. Epub 20211223. doi: 10.1038/s41396-021-01179-3.
962 PMID: 34949784.
963 68. Gordillo Altamirano FL, Barr JJ. Unlocking the next generation of phage therapy: the key
964 is in the receptors. Curr Opin Biotechnol. 2021;68:115-23. Epub 2020/11/18. doi:
965 10.1016/j.copbio.2020.10.002. PMID: 33202354.
966 69. Knezevic P, Curcin S, Aleksic V, Petrusic M, Vlaski L. Phage-antibiotic synergism: a
967 possible approach to combatting *Pseudomonas aeruginosa*. Res Microbiol. 2013;164(1):55-60.
968 Epub 2012/09/25. doi: 10.1016/j.resmic.2012.08.008. PMID: 23000091.
969 70. Luo J, Xie L, Liu M, Li Q, Wang P, Luo C. Bactericidal Synergism between Phage
970 YC#06 and Antibiotics: a Combination Strategy to Target Multidrug-Resistant *Acinetobacter*
971 *baumannii* In Vitro and In Vivo. Microbiol Spectr. 2022:e0009622. Epub 2022/06/24. doi:
972 10.1128/spectrum.00096-22. PMID: 35736241.
973 71. Furniss RCD, Kaderabkova N, Barker D, Bernal P, Maslova E, Antwi AAA, et al.
974 Breaking antimicrobial resistance by disrupting extracytoplasmic protein folding. Elife. 2022;11.
975 Epub 2022/01/14. doi: 10.7554/eLife.57974. PMID: 35025730.
976 72. Collet JF, Cho SH, Iorga BI, Goemans CV. How the assembly and protection of the
977 bacterial cell envelope depend on cysteine residues. J Biol Chem. 2020;295(34):11984-94. Epub
978 2020/06/04. doi: 10.1074/jbc.REV120.011201. PMID: 32487747.
979 73. Delhaye A, Laloux G, Collet JF. The Lipoprotein NlpE Is a Cpx Sensor That Serves as a
980 Sentinel for Protein Sorting and Folding Defects in the *Escherichia coli* Envelope. J Bacteriol.
981 2019;201(10). Epub 2019/03/06. doi: 10.1128/JB.00611-18. PMID: 30833359.
982 74. Danese PN, Silhavy TJ. The sigma(E) and the Cpx signal transduction systems control
983 the synthesis of periplasmic protein-folding enzymes in *Escherichia coli*. Genes Dev.
984 1997;11(9):1183-93. Epub 1997/05/01. doi: 10.1101/gad.11.9.1183. PMID: 9159399.
985 75. Pogliano J, Lynch AS, Belin D, Lin EC, Beckwith J. Regulation of *Escherichia coli* cell
986 envelope proteins involved in protein folding and degradation by the Cpx two-component
987 system. Genes Dev. 1997;11(9):1169-82. Epub 1997/05/01. doi: 10.1101/gad.11.9.1169. PMID:
988 9159398.

989 76. Hirano Y, Hossain MM, Takeda K, Tokuda H, Miki K. Structural studies of the Cpx
990 pathway activator NlpE on the outer membrane of *Escherichia coli*. Structure. 2007;15(8):963-
991 76. Epub 2007/08/19. doi: 10.1016/j.str.2007.06.014. PMID: 17698001.
992 77. Zhang G, Baidin V, Pahil KS, Moison E, Tomasek D, Ramadoss NS, et al. Cell-based
993 screen for discovering lipopolysaccharide biogenesis inhibitors. Proc Natl Acad Sci U S A.
994 2018;115(26):6834-9. Epub 2018/05/08. doi: 10.1073/pnas.1804670115. PMID: 29735709.
995 78. Robinson JT, Thorvaldsdottir H, Winckler W, Guttman M, Lander ES, Getz G, et al.
996 Integrative genomics viewer. Nat Biotechnol. 2011;29(1):24-6. Epub 2011/01/12. doi:
997 10.1038/nbt.1754. PMID: 21221095.
998 79. McCoy KM, Antonio ML, van Opijnen T. MAGenTA: a Galaxy implemented tool for
999 complete Tn-Seq analysis and data visualization. Bioinformatics. 2017;33(17):2781-3. Epub
1000 2017/05/13. doi: 10.1093/bioinformatics/btx320. PMID: 28498899.
1001 80. Kropinski AM, Mazzocco A, Waddell TE, Lingohr E, Johnson RP. Enumeration of
1002 bacteriophages by double agar overlay plaque assay. Methods Mol Biol. 2009;501:69-76. Epub
1003 2008/12/11. doi: 10.1007/978-1-60327-164-6_7. PMID: 19066811.
1004 81. Dai Y, Pinedo V, Tang AY, Cava F, Geisinger E. A New Class of Cell Wall-Recycling
1005 l,d-Carboxypeptidase Determines beta-Lactam Susceptibility and Morphogenesis in
1006 *Acinetobacter baumannii*. mBio. 2021;12(6):e0278621. Epub 2021/12/08. doi:
1007 10.1128/mBio.02786-21. PMID: 34872350.
1008 82. Deatherage DE, Barrick JE. Identification of mutations in laboratory-evolved microbes
1009 from next-generation sequencing data using breseq. Methods Mol Biol. 2014;1151:165-88. doi:
1010 10.1007/978-1-4939-0554-6_12. PMID: 24838886.
1011 83. Jolley KA, Bray JE, Maiden MCJ. Open-access bacterial population genomics: BIGSdb
1012 software, the PubMLST.org website and their applications. Wellcome Open Res. 2018;3:124.
1013 Epub 2018/10/23. doi: 10.12688/wellcomeopenres.14826.1. PMID: 30345391.
1014 84. Wyres KL, Cahill SM, Holt KE, Hall RM, Kenyon JJ. Identification of *Acinetobacter*
1015 *baumannii* loci for capsular polysaccharide (KL) and lipooligosaccharide outer core (OCL)
1016 synthesis in genome assemblies using curated reference databases compatible with Kaptive.
1017 Microb Genom. 2020;6(3). Epub 2020/03/03. doi: 10.1099/mgen.0.000339. PMID: 32118530.
1018 85. Hua X, Liang Q, Fang L, He J, Wang M, Hong W, et al. Bautype: Capsule and
1019 Lipopolysaccharide Serotype Prediction for *Acinetobacter baumannii* Genome. Infectious
1020 Microbes & Diseases. 2020;2(1):18-25. doi: 10.1097/im9.0000000000000019. PMID:
1021 02123149-202003000-00004.
1022 86. Gao R, Stock AM. Probing kinase and phosphatase activities of two-component systems
1023 in vivo with concentration-dependent phosphorylation profiling. Proc Natl Acad Sci U S A.
1024 2013;110(2):672-7. Epub 2012/12/26. doi: 10.1073/pnas.1214587110. PMID: 23267085.
1025 87. Marchler-Bauer A, Bo Y, Han L, He J, Lanczycki CJ, Lu S, et al. CDD/SPARCLE:
1026 functional classification of proteins via subfamily domain architectures. Nucleic Acids Res.
1027 2017;45(D1):D200-D3. Epub 2016/12/03. doi: 10.1093/nar/gkw1129. PMID: 27899674.
1028 88. Almagro Armenteros JJ, Tsirigos KD, Sonderby CK, Petersen TN, Winther O, Brunak S,
1029 et al. SignalP 5.0 improves signal peptide predictions using deep neural networks. Nat
1030 Biotechnol. 2019;37(4):420-3. Epub 2019/02/20. doi: 10.1038/s41587-019-0036-z. PMID:
1031 30778233.
1032

1033 **Captions**

1034 **Fig 1. Identification of candidate determinants of susceptibility to Loki using Tn-seq.**

1035 (A) Loki infection of *A. baumannii* 17978 causes partial inhibition of bulk culture growth.
1036 Bacteria were seeded in microplates with or without Loki at the indicated MOI and growth was
1037 monitored by OD readings (liquid infection assay). Data points show geometric mean ± s.d.
1038 (shaded bands) from n = 3 independent cultures. Where not visible, s.d. is within the confines of
1039 the symbol. Inset shows small, turbid plaques resulting from Loki infection of the same strain on
1040 solid medium. Plaques imaged with white light transillumination. Scale bar, 1 mm. (B) Tn-seq
1041 analysis of Loki susceptibility determinants in *A. baumannii* 17978. Volcano plots show change
1042 in gene-level fitness resulting from phage treatment at the indicated MOI compared to untreated
1043 control, plotted against inverse p value from parallel t tests. Blue data points are genes that pass
1044 significance criteria (Materials and Methods) and represent candidate Loki susceptibility
1045 determinants. Loci described further in the text are labelled. Grey data points are genes not
1046 passing significance criteria.

1047

1048 **Fig 2. Validation of candidate phage hypersusceptibility loci.**

1049 (A) Tracks show Tn-seq fitness values (vertical bars) of individual *Mariner* transposon mutants
1050 at candidate Loki hypersusceptibility loci (shaded yellow) across all tested mutant banks using
1051 the indicated MOI. (B-C) Liquid challenge assays with defined mutants. Growth of the indicated
1052 *A. baumannii* 17978 strains with Loki (MOI 1) or no phage was measured as in Fig 1A (n=3).
1053 "Chr" indicates the chromosomal mutation; "Plasmid" denotes the gene reintroduced under
1054 P(IPTG) control via vector pYDE152; - indicates control plasmid with no reintroduced gene;
1055 *bfmS** refers to *bfmS*-null point mutant EGA127; IPTG "0.1" and "1" refer to mM units. (D-E)

1056 Plaque formation assays. ~10^8 of the indicated bacteria were overlaid on bottom agar, followed
1057 by spotting 10-fold serial dilutions of Loki. Bottom agar in D contained 1mM IPTG. Plaques
1058 were imaged with white-light transillumination after 16 h incubation at 30°C.
1059
1060 **Fig 3. Loki resistance mutations map to capsule biosynthesis locus.** (A) Tn-seq fitness of
1061 transposon mutants in the capsule synthesis (KL3) and associated loci in the Loki challenge
1062 screen. Plotted are the average gene-level Tn-seq fitness values (*W*) with phage infection (Loki
1063 MOI 10-15) vs uninfected control, analyzed by unpaired t-tests. X indicates essential gene
1064 without a fitness value due to paucity of transposon insertions. Dotted line indicates the genome-
1065 wide average *W* during Loki challenge. (B-C, E) Plaque formation assays showing dependence
1066 on the KL3 capsule for Loki infection. Loki was spotted on the following hosts: (B) acapsular
1067 *itrA* and *wzc* mutants of 17978; (C) a range of *A. baumannii* clinical isolates harboring the
1068 indicated K and OC locus (K loci producing the K3 capsule type are shaded blue); or (E) strains
1069 with spontaneous *gtr6* mutations (Table S1). Strains in E harbored the indicated pYDE152-based
1070 plasmid and bottom agar contained 1mM IPTG. (D) Diagram of the KL3/KL22 cluster showing
1071 spontaneous Loki resistance mutations (arrowheads). The hotspot within *gtr6* is expanded. KL3
1072 and KL22 share all ORFs except *pgt1* (only present in KL22).
1073
1074 **Fig 4. Results of phage adsorption assays measuring *A. baumannii* binding to Loki.** Loki
1075 adsorption assays were performed with WT 17978 or the indicated mutant. Data points show
1076 geometric mean ± s.d. (n=3), analyzed by unpaired t test (mutant vs WT control). P values: *,
1077 ≤0.05; **, ≤0.01; ***, <0.001; ns, not significant.
1078

1079 **Fig. 5. Susceptibility to Loki depends on BfmRS activity and correlates with control of**
1080 **capsule levels.**
1081 (A) *bfmS* and *bfmR* transposon mutations have opposing effects on Tn-seq fitness during Loki
1082 challenge. Data points show average gene-level Tn-seq fitness values (*W*) with Loki infection at
1083 indicated MOI vs uninfected control, analyzed by unpaired t-tests. Dotted line indicates the
1084 genome-wide average *W* during Loki challenge (MOI 10-15). (B) Capsule production by
1085 different *bfmRS* mutants. Bars show mean capsule level ± s.d. (n=3), analyzed by one-way
1086 ANOVA with Dunnett's multiple comparisons test (mutant vs WT). A representative gel is
1087 shown above the graph. (C) Liquid challenge and (D) plaque formation assays with Δ*bfmRS* and
1088 *bfmR* receiver domain point mutants. Liquid challenge data are presented as in Fig 1A (n=3). (E)
1089 BfmR phosphorylation level was analyzed in cell lysates of receiver domain mutants vs the
1090 parent control (*bfmS**) by Phos-tag western blotting. BfmR~P as a fraction of total BfmR was
1091 quantified from n=3 samples. Bars show mean ± s.d., analyzed by one-way ANOVA with
1092 Tukey's multiple comparisons test. A representative blot is shown above the graph.
1093
1094 **Fig 6. RnaA and DsbA modulate capsule production and Loki susceptibility through**
1095 **BfmRS and in different clinical isolates.**
1096 (A) Capsule levels measured in 17978 derivatives with Δ*rnaA* and Δ*dsbA* mutation singly and in
1097 combination with Δ*bfmRS*. A representative gel (top) and quantification from n=3 samples
1098 (bottom; means ± s.d. analyzed by one-way ANOVA with Šídák's multiple comparisons test) are
1099 shown as in Fig 5B. (B) Liquid challenge assays examining susceptibility of strains in A to Loki
1100 attack. Data presented as in Fig 1A (n=6). (C-D) Δ*rnaA* and Δ*dsbA* derivatives of carbapenem-
1101 resistant *A. baumannii* strain BAA-1790 show increased capsule and Loki sensitivity. Capsule

1102 levels (C) were analyzed as in A. Bacterial growth during liquid challenge with a virulent Loki
1103 derivative (Loki*) (D) was analyzed as in B. (E-F) *rnaA* overexpression via high-copy plasmid
1104 decreases capsule production and blocks Loki infection in a manner dependent on the BfmS
1105 signal receptor. WT or *bfmS** 17978 bacteria harbored pJE127 (IPTG-dependent *rnaA*) and were
1106 grown in the presence or absence of IPTG. Representative capsule gel (E, top), capsule
1107 quantification from n=3 samples (E, bottom), and Loki plaque assays (F) are shown. Mean
1108 capsule levels ± s.d. were analyzed by unpaired t-tests. P values: *, ≤0.05; **, ≤0.01; ***,
1109 <0.001. ns, not significant.
1110
1111 **Fig 7. RnaA/DsbA deficiency activates BfmRS.**
1112 (A) Transcription levels of capsule biosynthesis genes *wza* (black) and *gnaA* (gray) measured by
1113 qRT-PCR in Δ*rnaA* and Δ*dsbA* mutants. Bars show mean fold change vs WT ± s.d. (n=3);
1114 analyzed by unpaired t-tests comparing mutant vs WT. (B-C) Fluorescence reporter assays.
1115 Strains harbored a GFP transcriptional fusion to the noted promoter region and reporter
1116 fluorescence was measured as fluorescence units/A_{600}. (B) Δ*rnaA* and Δ*dsbA* activation of a
1117 BfmRS-dependent (*18040*p, black), but not BfmRS-independent (*adc*p, gray) promoter. (C)
1118 Δ*rnaA*/Δ*dsbA* activation of *18040*p requires BfmRS. Bars show mean ± s.d. (n = 3). Means were
1119 analyzed by unpaired t test comparing mutant vs WT (B) or by one-way ANOVA with Šídák's
1120 multiple comparisons test (C). (D) Phos-tag analysis of BfmR phosphorylation. Δ*rnaA* and
1121 Δ*dsbA* increase BfmR~P to a level matching that caused by the hyperactive Δ*bfmS* allele.
1122 Presented as in Fig 5E (n=3). Asterisks show results of one-way ANOVA with Tukey's multiple
1123 comparisons test (mutant vs WT); comparisons between mutants were not significant. (E) Heat
1124 map shows the Pearson correlation coefficients (r) analyzing relatedness of Tn-seq phenotypic

1125 signatures [41] of *bfmS, rnaA,* and *dsb* genes. (F) Tn-seq fitness of *rnaA* and *dsb* transposon
1126 mutants in the phage challenge screen. Data presented as in Fig 5A. (G) Δ*dsbA* but not Δ*rnaA*
1127 shows a synthetic growth defect with Δ*bfmRS.* Bacteria were incubated in LB at 37°C and
1128 growth measured as in Fig 1A (n=3). P values: *, ≤0.05; **, ≤0.01; ***, <0.001. ns, not
1129 significant.
1130
1131 **Fig 8. The full-length LOS outer core impedes attack by Loki independent of changes to**
1132 **capsule.**
1133 (A) Δ*gtrOC3* and Δ*gtrOC4* cause enrichment of a truncated LOS intermediate. A representative
1134 LOS gel (top) and quantification from triplicate samples (bottom) are shown. Bars indicate mean
1135 normalized LOS levels ± s.d.; one-way ANOVA showed no significant difference in total LOS
1136 levels among strains (P=0.34). (B) Tn-seq fitness of LOS outer core synthesis locus (OCL2)
1137 mutants in the phage challenge screen. Data presented as in Fig 3A. (C-D) Enhancement of Loki
1138 susceptibility in *gtrOC* mutants depends on capsule. (C) Plaque formation assay with Δ*gtrOC3,*
1139 Δ*itrA*, Δ*gtr6*, and double mutants. (D) Liquid challenge assay with strains in C (n = 3). P values:
1140 *, ≤0.05; **, ≤0.01; ***, <0.001. ns, not significant.
1141
1142 **Fig. 9. Model for modulation of phage infection by multiple susceptibility factors in *A.***
1143 ***baumannii*.** Vulnerability factors that act to enhance Loki infection are shown in blue; defense
1144 factors that antagonize Loki infection are shown in red. Additional candidate defense factors,
1145 including the methyltransferase AamA or transcription factor DksA, were identified through
1146 screening but require confirmation and are not shown. (A) Loki infection of WT bacteria. Loki
1147 adsorbs in two steps: (1) interaction with the primary adsorption receptor, capsular

1148 polysaccharide of type K3, and (2) interaction with an LOS-associated secondary site. This site
1149 may be the conserved LOS inner core, or LOS-proximal capsule residues, and access is
1150 antagonized by the LOS outer core. BfmRS enhances Loki infection by positively regulating
1151 both the capsule receptor (via transcriptional activation of capsule biosynthesis) and intracellular
1152 phage replication (by unknown mechanisms). Lon protease negatively regulates intracellular
1153 phage replication, by unknown mechanisms. (B) Loki resistance arises from capsule receptor
1154 down-regulation (BfmRS deficiency), structural alteration (via mutation of hotspot gene *gtr6*), or
1155 complete loss (mutation of a core biosynthesis gene, e.g. *itrA* or *wzx*), blocking phage adsorption.
1156 BfmRS deficiency may also reduce phage intracellular replication. (C) By contrast, Loki
1157 hypersusceptibility arises from hyperactivity of vulnerability factors or loss of defense factors.
1158 Hyperactivation of BfmRS, defined by increased BfmR~P (yellow halo), results from *bfmS*,
1159 *dsbA*, or *rnaA* mutations and may also be triggered by external stresses related to oxidative
1160 protein folding. BfmRS hyperactivity increases the level of the capsule receptor, enhancing
1161 phage adsorption, while also stimulating phage intracellular multiplication. Loss of LOS OC
1162 sugars increases binding of Loki to surface sites without altering its intracellular multiplication.
1163 Loss of Lon increases phage multiplication without increasing adsorption.
1164

1165 **Supporting information captions**

1166 **S1 Fig. Analysis of phenotypes connected to *rnaA* and DSB genes.** (A) Liquid Loki challenge
1167 assays show that overexpression of reintroduced *rnaA* by a high inducer concentration (1mM
1168 IPTG) not only reverses the Δ*rnaA* phage susceptibility defect, but causes complete non-
1169 susceptibility to the phage. "Chr" indicates the chromosomal mutation; "Plasmid" denotes the
1170 gene reintroduced under P(IPTG) control via vector pYDE152; - indicates vector with no

1171 reintroduced gene. Bacteria were cultured with or without Loki (MOI 1) and IPTG (1mM) as
1172 indicated. Data are presented as in Fig. 1A (n=3). (B) Complementation analysis showing
1173 reversibility of capsule deficiency in Δ*rnaA* and Δ*dsbA* strains. Capsular polysaccharide levels
1174 were analyzed by SDS-PAGE/Alcian Blue after growth with the noted amount of IPTG to induce
1175 the reintroduced gene. (C-D) Plaque formation assays. Loki was spotted onto bottom agar
1176 containing WT bacteria with the indicated genotype. In D, bacteria harbored pJE101 (IPTG-
1177 dependent *dsbA*), and plates contained 0 or 1mM IPTG. (E) Cluster analysis of Tn-seq
1178 phenotypic signatures of *bfmS*, *rnaA*, and *dsb* genes. Heat map shows normalized Tn-seq fitness
1179 in z-score units for transposon mutants in each gene (rows) grown in different conditions
1180 (columns) [41]. Dendrogram at left shows relationship between signatures based on hierarchical
1181 clustering. (F) Heat map shows change in RNA-seq transcript levels in the indicated BfmRS
1182 mutant compared to WT control. Data were extracted from previous datasets [35] and log2 fold
1183 change values displayed as heat map using Prism 9. P values: *, ≤0.05; **, ≤0.01; ***, <0.001.
1184
1185 **S2 Fig. Analysis of Δ*slt* phenotypes.** (A) Liquid challenge assay with WT or Δ*slt* bacteria
1186 cultured with or without Loki (MOI 1). Data are presented as in Fig. 1A (n=3). (B) Plaque
1187 formation assay with Loki spotted onto bottom agar with WT and Δ*slt* bacteria. (C)
1188 Measurement of *rnaA* transcript levels in WT vs Δ*slt* via qRT-PCR. Bars show mean fold change
1189 vs WT ± s.d. (n = 3); analyzed by unpaired t-test. *, P ≤ 0.05.
1190
1191 **S3 Fig. Reintroduction of *itrA* in Δ*itrA* mutant restores Loki susceptibility in the liquid**
1192 **challenge assay, and degree of susceptibility increases with increasing *itrA* induction.** (A)
1193 Bacteria of the noted genotype were cultured with the indicated level of IPTG with or without

1194 Loki at initial MOI of 1. Growth was measured as in Fig 1A (n = 3). (B) Plaque formation assay
1195 with Loki spotted on 17978 WT and isogenic Δ*gtr6* mutant.
1196
1197 **S4 Fig. *gtr6*, *gtrOC*, and *lon* mutations do not affect production of capsular polysaccharide.**
1198 Bars show mean capsule levels ± s.d. (n=3). Lanes from representative gels are shown above
1199 each graph. No significant difference among means by one-way ANOVA (A, P = 0.797; B, P =
1200 0.963) or by t test (C, P = 0.531).
1201
1202 **S5 Fig. Analysis of total BfmR levels in mutant strains.** Total BfmR levels were quantified
1203 from anti-BfmR Phos-tag western blots by combining the signal from phosphorylated and
1204 unphosphorylated forms of BfmR, and normalizing to total protein in the sample as determined
1205 by SYPRO Ruby staining. (A) Graph corresponds to the blot shown in Fig. 5E. (B) Graph
1206 corresponds to the blot shown in Fig. 7D. Bars show mean capsule level ± s.d. (n=3), analyzed
1207 by one-way ANOVA with Dunnett's multiple comparisons test (mutant vs WT). *, P value ≤
1208 0.05.
1209
1210 **S6 Fig. *bfmS* and *gtrOC* mutant hypersusceptibility to Loki depends on capsule**
1211 **biosynthesis.** (A, D) Phage adsorption assays showing that enhancement of Loki adsorption by
1212 *bfmS* (A) or *gtrOC3* (D) mutations depends on capsule. Data presented as in Fig. 4 (n=3). (B)
1213 Liquid challenge assays. The indicated bacteria were cultured with or without Loki (MOI 1).
1214 Data are presented as in Fig 1A (n=3). (C) Plaque formation assays with Loki spotted on *A.*
1215 *baumannii* strains, and their corresponding *bfmS*-null derivative, harboring the indicated K locus.
1216

1217 **S7 Fig. Liquid phage challenge assays using *A. baumannii* strains BAA-1790 and 17978 and**
1218 **phages Loki or Loki*.** (A) The indicated BAA-1790 mutant, or WT control, was challenged
1219 with Loki. (B) 17978 WT was challenged with Loki, virulent Loki* derivative, or no phage
1220 control. Data points show geometric mean ± s.d. (n=3).
1221
1222 **S8 Fig. *A. baumannii* RnaA lacks catalytic residues defining the RNase T2 family.**
1223 Diagram shows analysis of conserved domains on RnaA. RNase_T2 domain, CAS motifs, and
1224 active site positions were identified using the NCBI Conserved Domain Database [87]. Signal
1225 peptide was identified using SignalP [88]. Vertical green lines represent conserved cysteine
1226 residues within the RNase_T2 domain. Alignment shows RNase T2 family homologs across
1227 diverse bacterial species. Within the conserved active site motifs (CAS-I and CAS-II), the active
1228 sites are indicated by #, and the most commonly found residues at these sites are highlighted.
1229
1230 **S9 Fig. Analysis of LOS production in altered phage susceptibility mutants bearing**
1231 **mutations in capsule-control loci or *lon*.** LOS production in cell lysates of mutants in *bfmRS*
1232 (A), *rnaA* and *dsbA* (B), and *lon* (C) was analyzed in comparison with WT control via Pro-Q 300
1233 emerald staining. Representative gels are shown in top panels. Arrowhead indicates location of
1234 novel intermediate band associated with Δ*bfmS* (A). Quantification is shown in bottom panels.
1235 Bars show mean ± s.d. (n=3). Within each set of strains, no significant difference ($P > 0.05$)
1236 observed in total LOS levels by one-way ANOVA (A, B) or unpaired t-test (C).
1237

1238 **S10 Fig. One-step growth curves showing enhanced Loki multiplication in phage**

1239 **hypersensitive mutant hosts.** Data points show geometric mean PFU/ml ± s.d. (n=4). Infected

1240 cell number (used in burst size calculations) was approximately 1-1.5 x 10^4 per ml.

1241

1242 **S1 Table. Strains, plasmids, and primers used in this study.**

1243

1244 **S2 Table. Spontaneous *gtr6* mutations conferring phage Loki resistance.**

1245

1246 **S1 Dataset. Loki challenge Tn-seq data.**

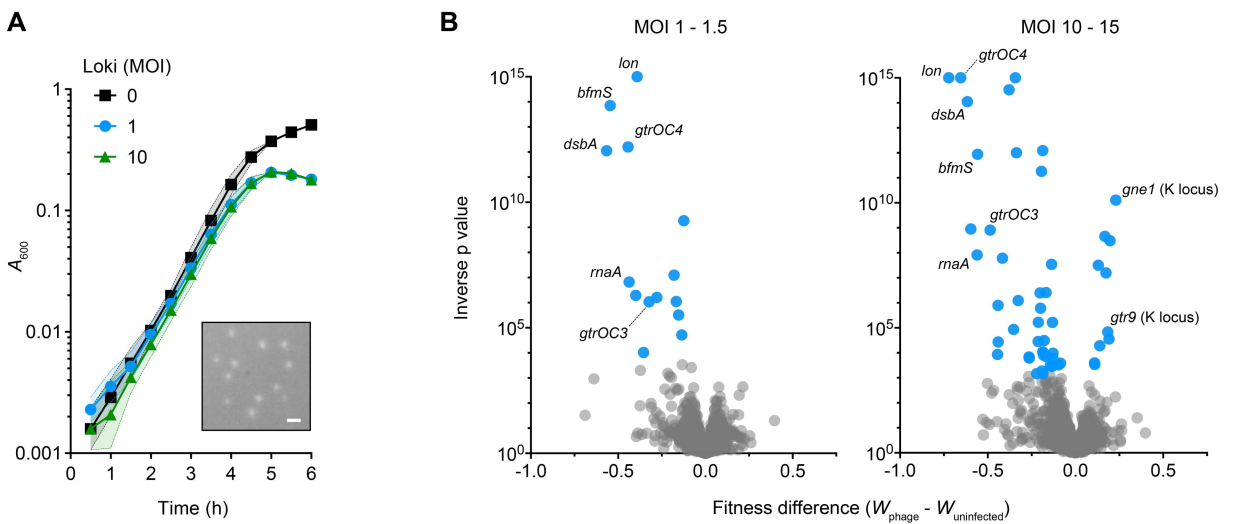
A
Loki (MOI)
0
1
10
A_{600}
1
0.1
0.01
0.001
0
1
2
3
4
5
6
Time (h)
B
MOI 1 - 1.5
MOI 10 - 15
Inverse p value
10^{15}
10^{10}
10^{5}
10^{0}
lon
bfmS
dsbA
gtrOC4
rnaA
gtrOC3
gne1 (K locus)
gtr9 (K locus)
-1.0
-0.5
0.0
0.5
Fitness difference (W_{phage} - $W_{uninfected}$)

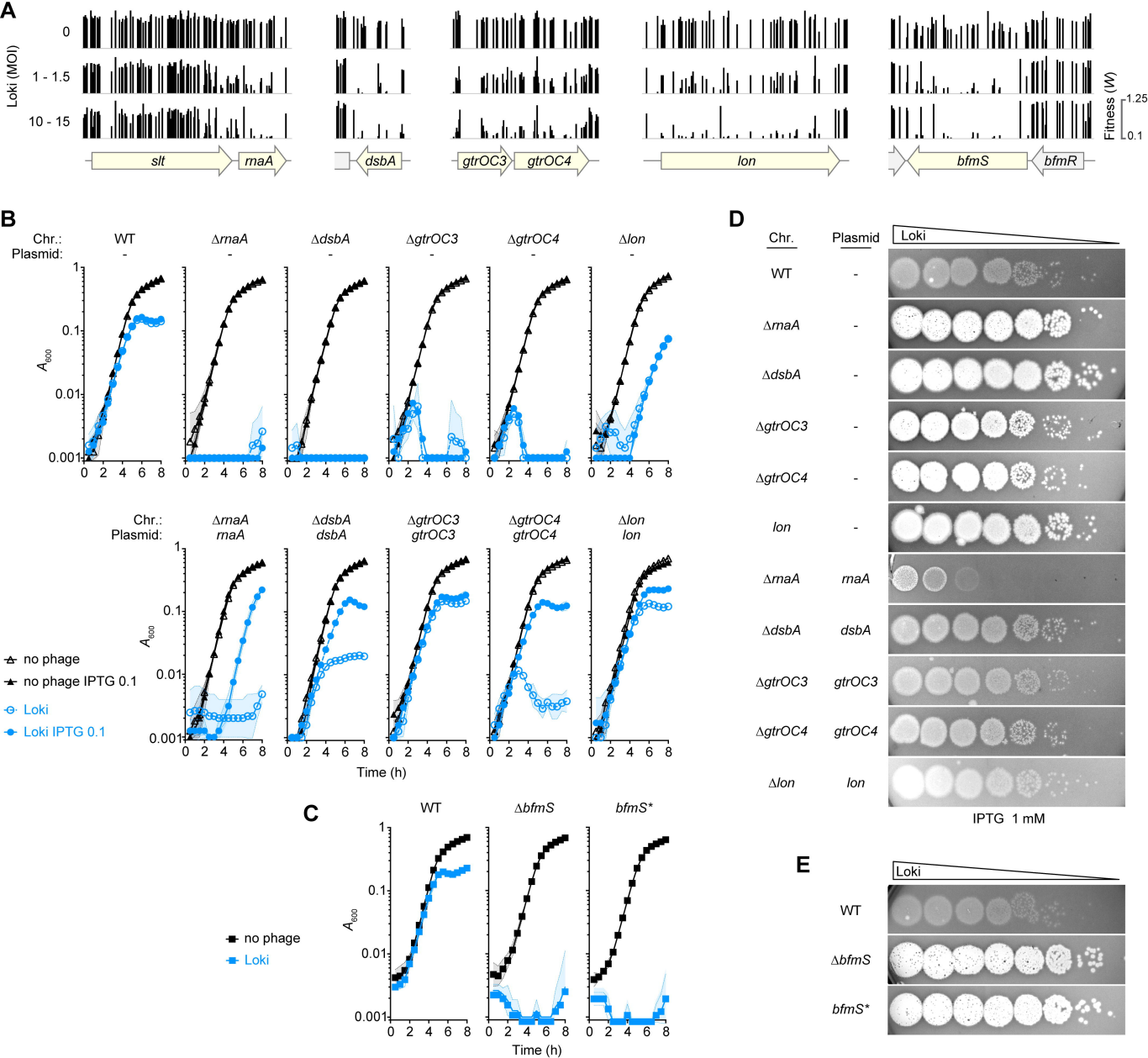
A
Loki (MOI)
0
1 - 1.5
10 - 15
Fitness (W)
1.25
0.1
slt
rnaA
dsbA
gtrOC3
gtrOC4
lon
bfmS
bfmR
B
Chr.:
Plasmid:
WT
ΔrnaA
ΔdsbA
ΔgtrOC3
ΔgtrOC4
Δlon
A600
Time (h)
no phage
no phage IPTG 0.1
Loki
Loki IPTG 0.1
C
ΔbfmS
bfmS*
D
Chr.
Plasmid
Loki
IPTG 1 mM
E

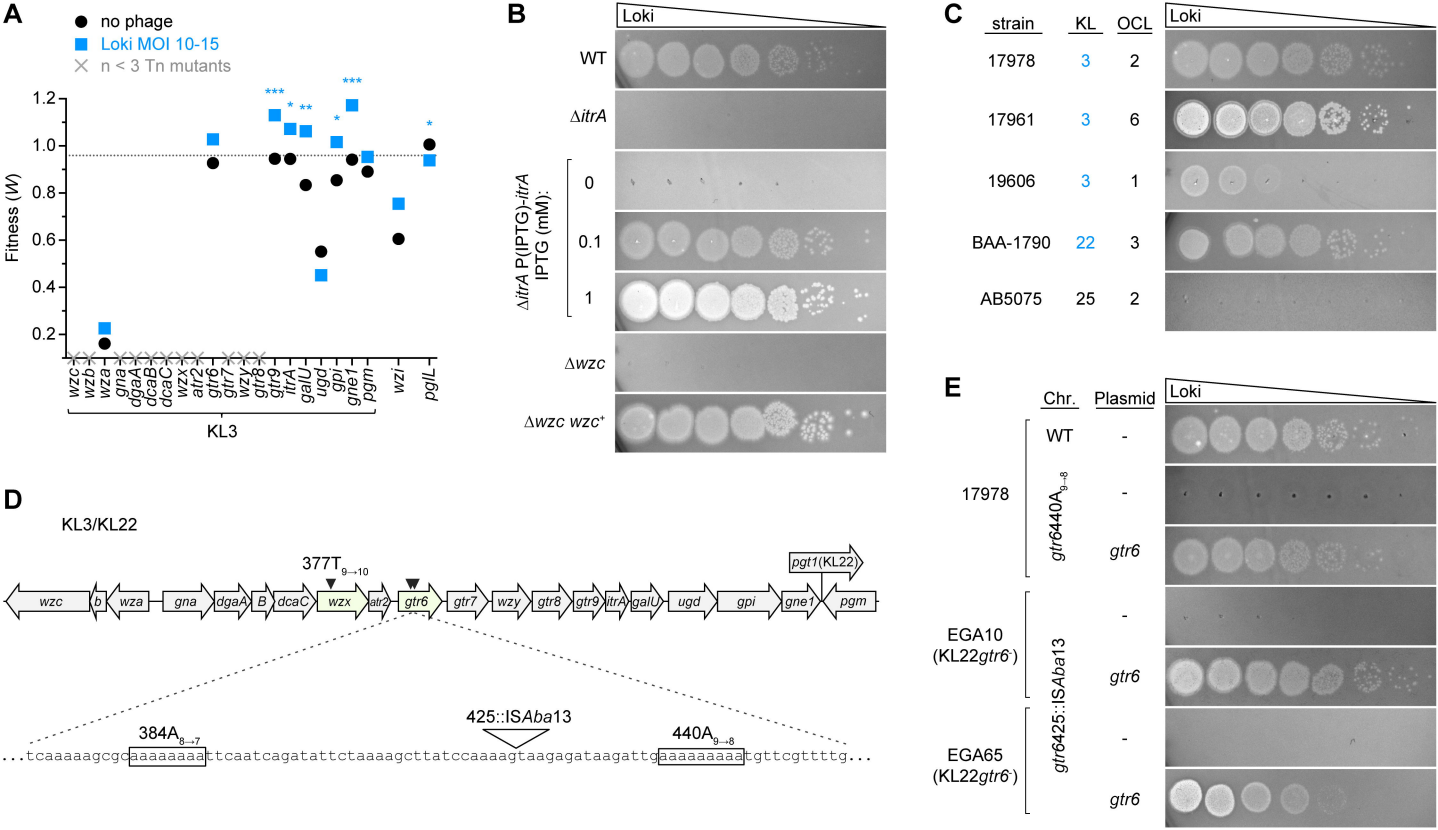
A
no phage
Loki MOI 10-15
n < 3 Tn mutants
Fitness (W)
1.2
1.0
0.8
0.6
0.4
0.2
wzc
wzb
wza
gna
dgaA
dcaB
dcaC
wzx
atr2
gtr6
gtr7
wzy
gtr8
gtr9
itrA
galU
ugd
gpi
gne1
pgm
wzi
pglL
KL3
B
Loki
WT
ΔitrA
ΔitrA P(IPTG)-itrA
IPTG (mM):
0
0.1
1
Δwzc
Δwzc wzc+
C
strain
KL
OCL
17978
3
2
17961
3
6
19606
3
1
BAA-1790
22
3
AB5075
25
2
Loki
D
KL3/KL22
377T9→10
pgt1(KL22)
wzc
b
wza
gna
dgaA
B
dcaC
wzx
atr2
gtr6
gtr7
wzy
gtr8
gtr9
itrA
galU
ugd
gpi
gne1
pgm
384A8→7
425::ISAba13
440A9→8
...tcaaaaagcgcaaaaaaaacttcaatcagatattctaaaagcttatccaaaagtaagagataagattgaaaaaaaatgttcgttttg...
E
Chr.
Plasmid
Loki
17978
WT
-
gtr6440A9→8
-
gtr6
EGA10
(KL22gtr6-)
gtr6425::ISAba13
-
gtr6
EGA65
(KL22gtr6-)
-
gtr6

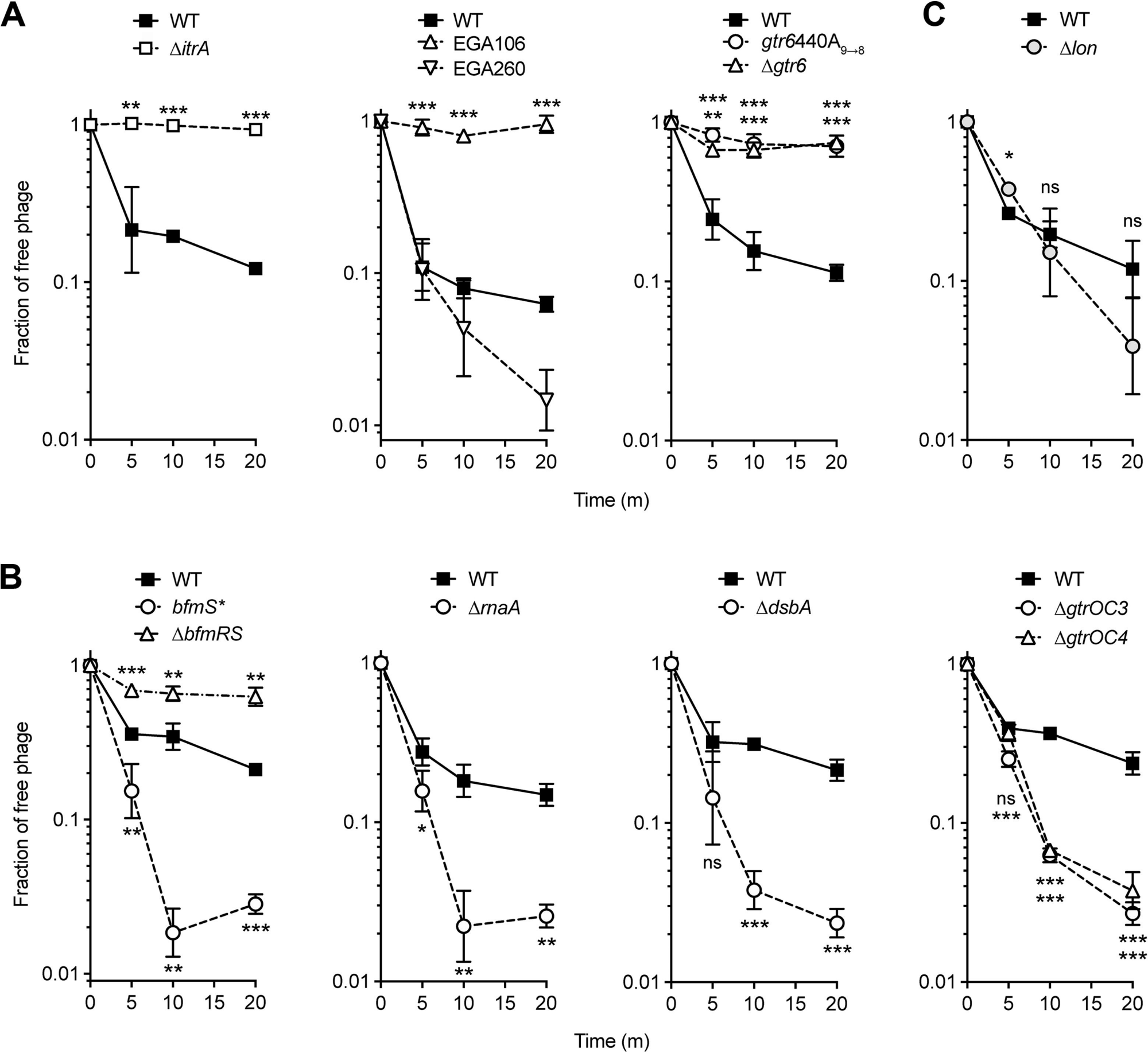
A
WT
ΔitrA
WT
EGA106
EGA260
WT
gtr6440A9→8
Δgtr6
C
WT
Δlon
Fraction of free phage
Time (m)
B
WT
bfmS*
ΔbfmRS
WT
ΔrnaA
WT
ΔdsbA
WT
ΔgtrOC3
ΔgtrOC4
Fraction of free phage
Time (m)

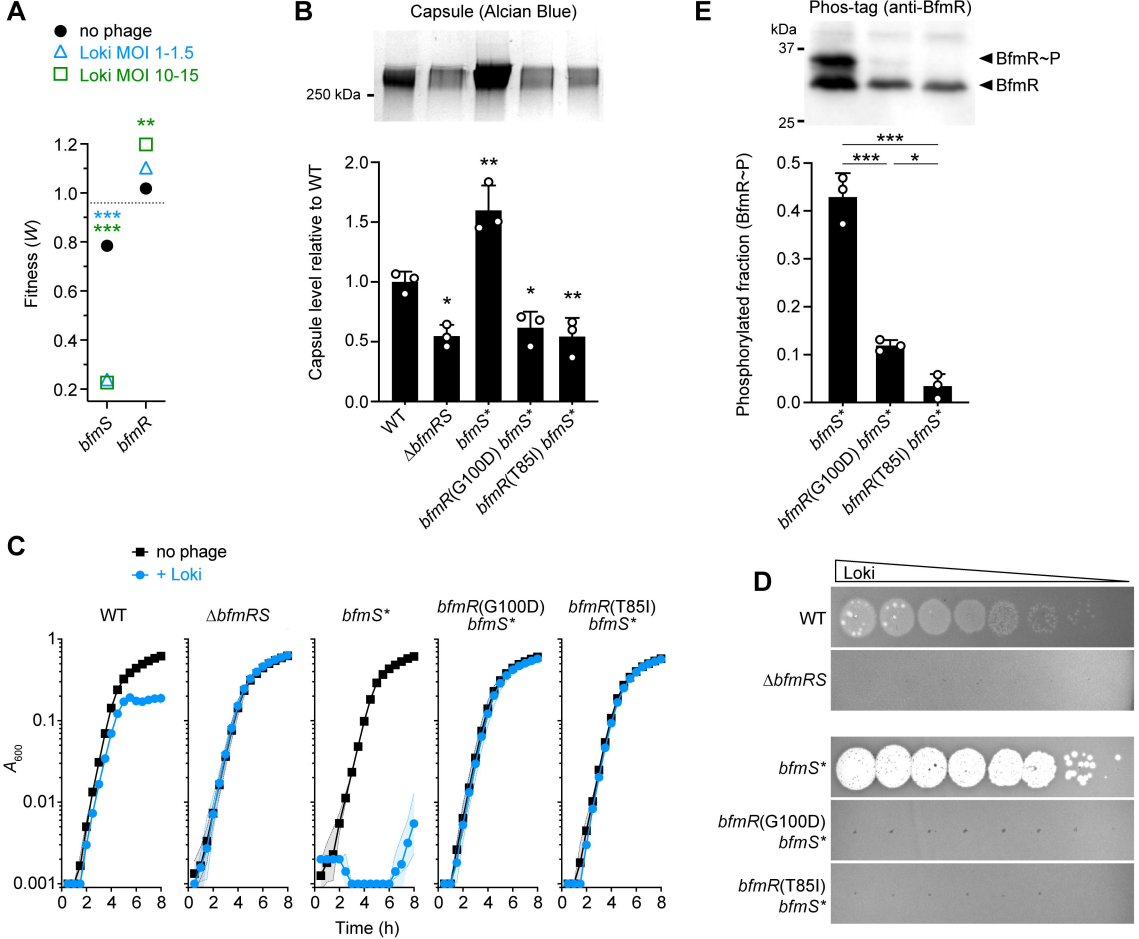
A
no phage
Loki MOI 1-1.5
Loki MOI 10-15
Fitness (W)
1.2
1.0
0.8
0.6
0.4
0.2
**
***
***
bfmS
bfmR
B
Capsule (Alcian Blue)
250 kDa
Capsule level relative to WT
2.0
1.5
1.0
0.5
0.0
**
*
*
**
WT
ΔbfmRS
bfmS*
bfmR(G100D) bfmS*
bfmR(T85I) bfmS*
E
Phos-tag (anti-BfmR)
kDa
37
25
BfmR~P
BfmR
Phosphorylated fraction (BfmR~P)
0.5
0.4
0.3
0.2
0.1
0.0
***
***
*
bfmS*
bfmR(G100D) bfmS*
bfmR(T85I) bfmS*
C
no phage
+ Loki
WT
ΔbfmRS
bfmS*
bfmR(G100D) bfmS*
bfmR(T85I) bfmS*
A600
1
0.1
0.01
0.001
0 2 4 6 8
Time (h)
D
Loki
WT
ΔbfmRS
bfmS*
bfmR(G100D) bfmS*
bfmR(T85I) bfmS*

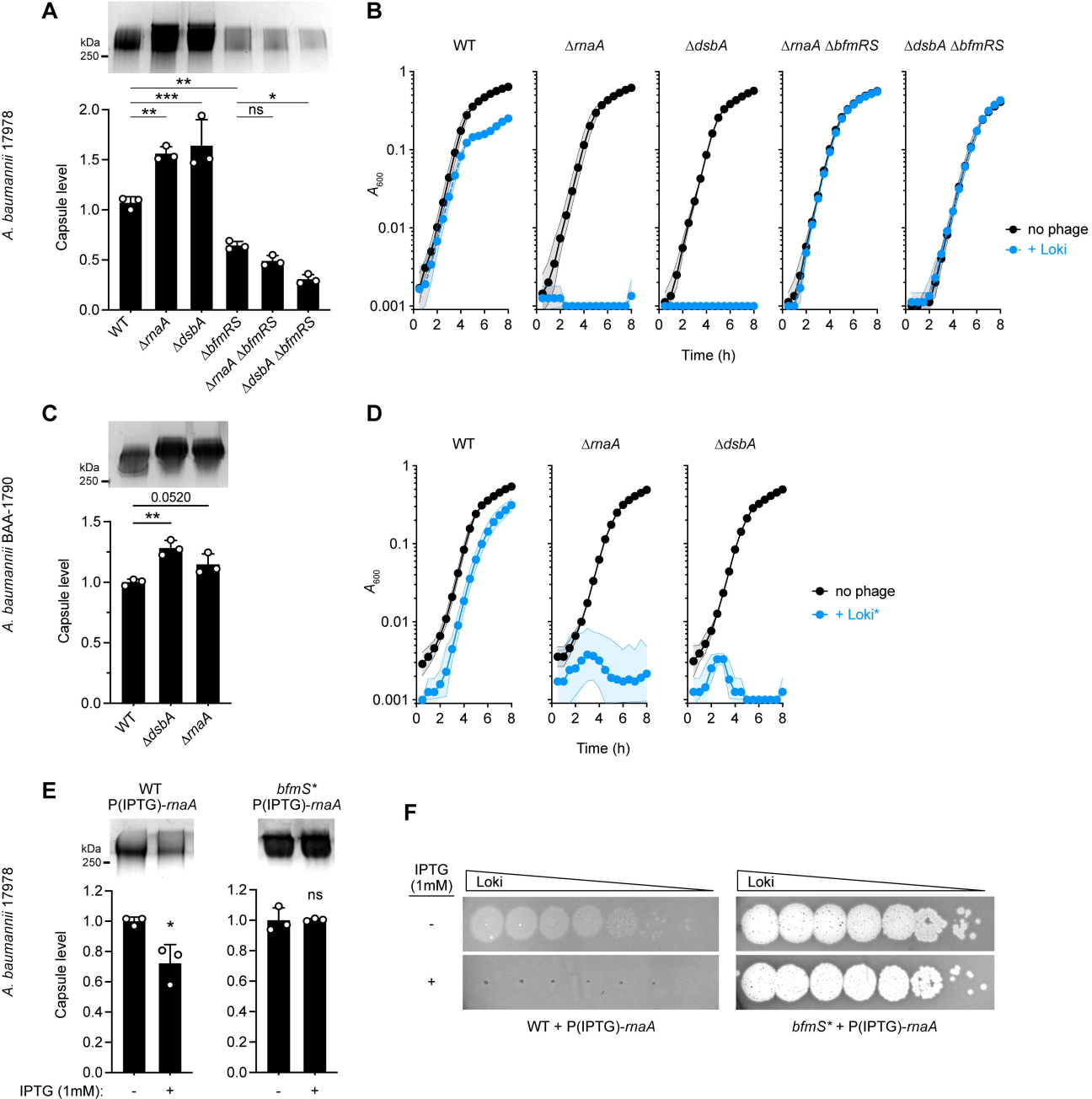
A
A. baumannii 17978
kDa
250
Capsule level
WT
ΔrnaA
ΔdsbA
ΔbfmRS
ΔrnaA ΔbfmRS
ΔdsbA ΔbfmRS
**
***
ns
*
B
WT
ΔrnaA
ΔdsbA
ΔrnaA ΔbfmRS
ΔdsbA ΔbfmRS
A600
Time (h)
no phage
+ Loki
C
A. baumannii BAA-1790
0.0520
D
+ Loki*
E
WT
P(IPTG)-rnaA
bfmS*
IPTG (1mM):
F
IPTG
(1mM)
Loki
WT + P(IPTG)-rnaA
bfmS* + P(IPTG)-rnaA

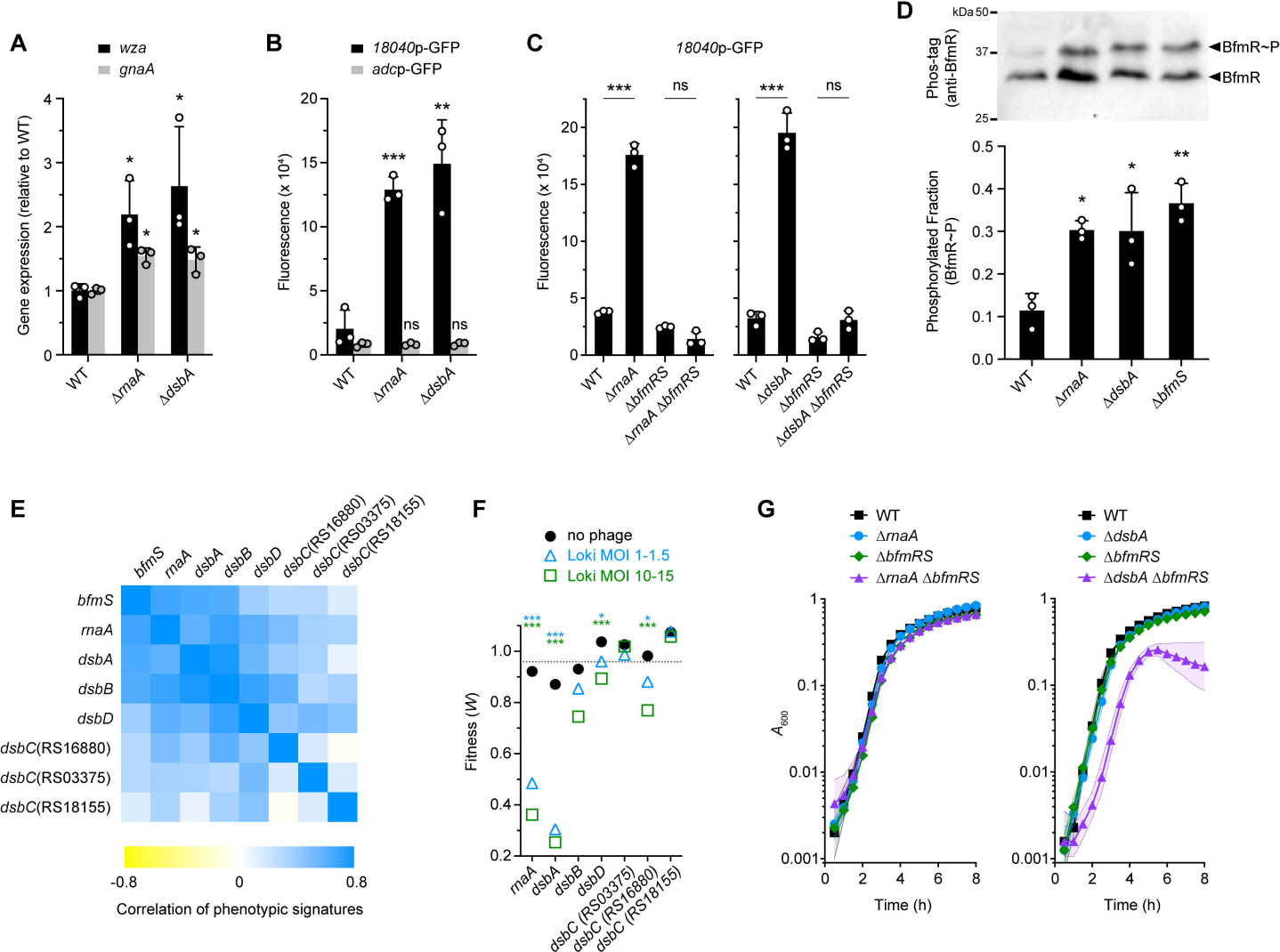
A
wza
gnaA
Gene expression (relative to WT)
WT
ΔrnaA
ΔdsbA
B
18040p-GFP
adcp-GFP
Fluorescence (x 10⁴)
ns
C
18040p-GFP
ΔbfmRS
ΔrnaA ΔbfmRS
ΔdsbA ΔbfmRS
D
kDa
Phos-tag (anti-BfmR)
BfmR~P
BfmR
Phosphorylated Fraction (BfmR~P)
ΔbfmS
E
bfmS
rnaA
dsbA
dsbB
dsbD
dsbC(RS16880)
dsbC(RS03375)
dsbC(RS18155)
Correlation of phenotypic signatures
F
no phage
Loki MOI 1-1.5
Loki MOI 10-15
Fitness (W)
G
WT
ΔrnaA
ΔbfmRS
ΔrnaA ΔbfmRS
ΔdsbA
ΔdsbA ΔbfmRS
A600
Time (h)

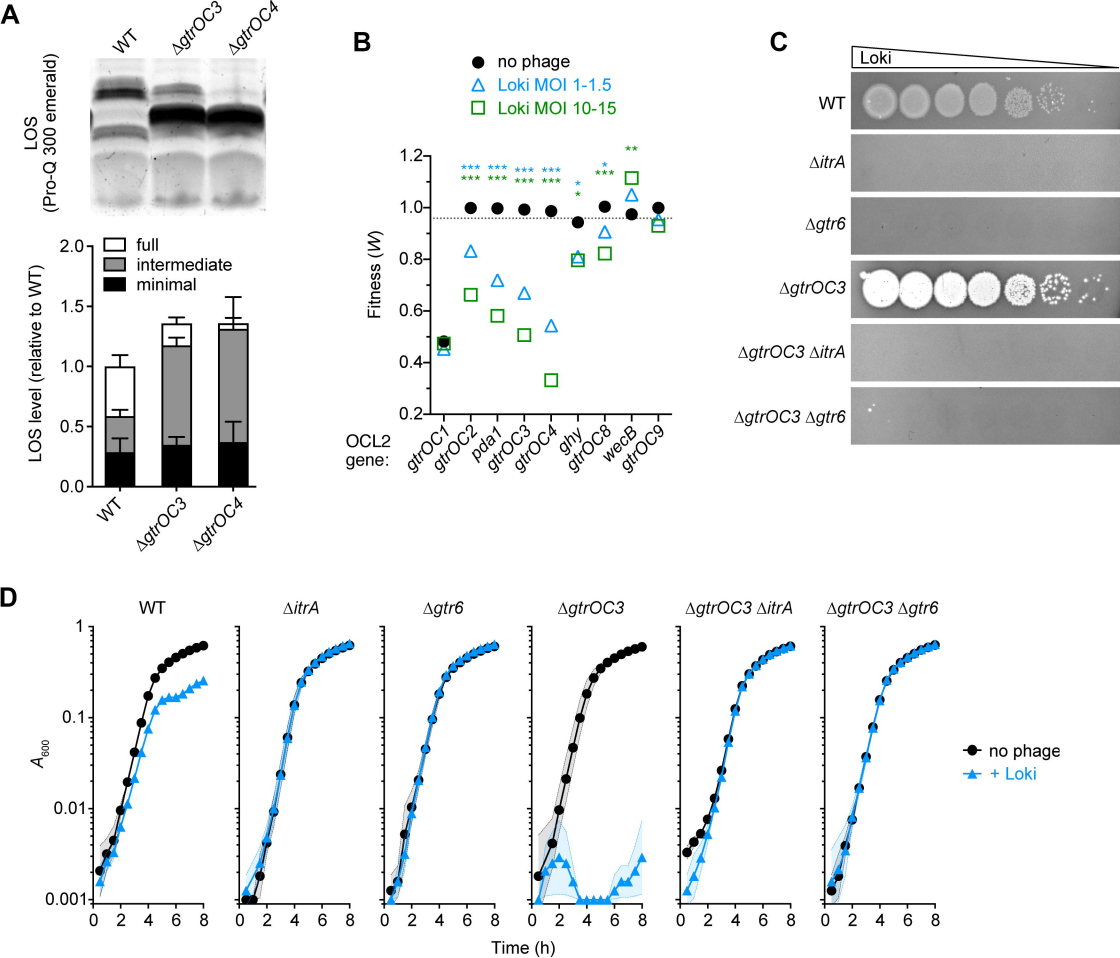
A
WT
ΔgtrOC3
ΔgtrOC4
LOS
(Pro-Q 300 emerald)
full
intermediate
minimal
LOS level (relative to WT)
2.0
1.5
1.0
0.5
0.0
WT
ΔgtrOC3
ΔgtrOC4
B
no phage
Loki MOI 1-1.5
Loki MOI 10-15
Fitness (W)
1.2
1.0
0.8
0.6
0.4
0.2
OCL2 gene:
gtrOC1
gtrOC2
pda1
gtrOC3
gtrOC4
ghy
gtrOC8
wecB
gtrOC9
C
Loki
WT
ΔitrA
Δgtr6
ΔgtrOC3
ΔgtrOC3 ΔitrA
ΔgtrOC3 Δgtr6
D
WT
ΔitrA
Δgtr6
ΔgtrOC3
ΔgtrOC3 ΔitrA
ΔgtrOC3 Δgtr6
A600
1
0.1
0.01
0.001
0
2
4
6
8
Time (h)
no phage
+ Loki

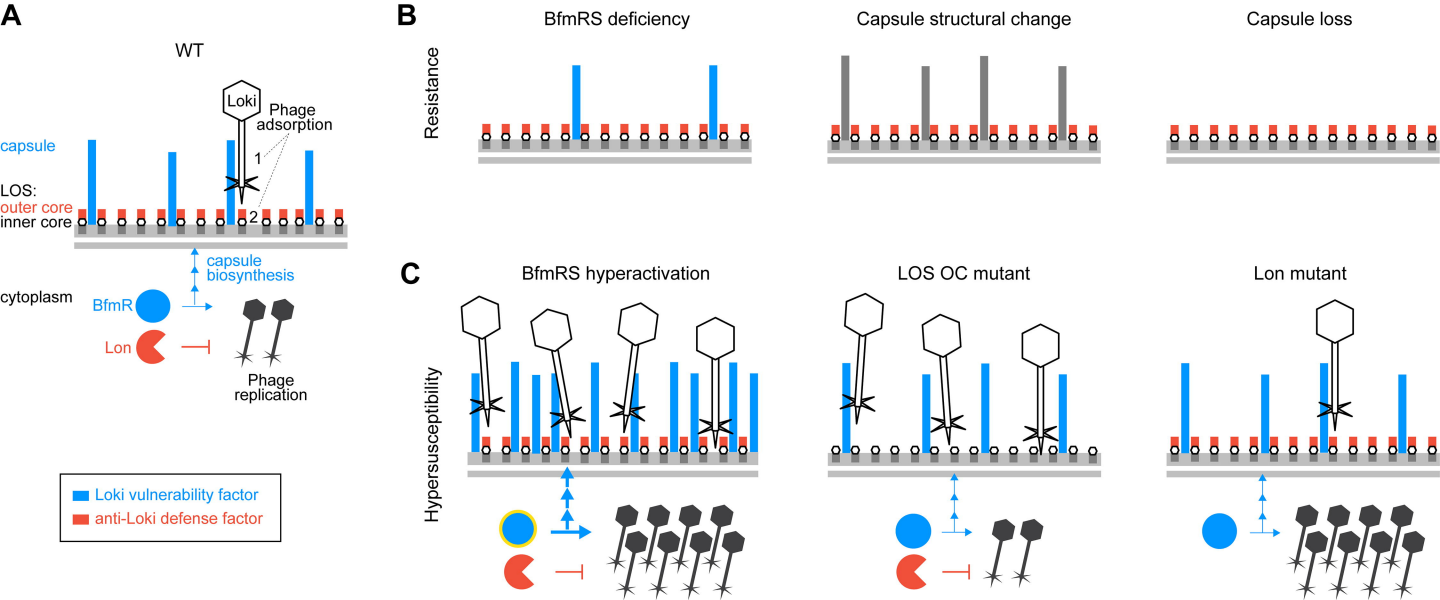
A
WT
Loki
Phage adsorption
capsule
1
LOS:
outer core
inner core
2
capsule biosynthesis
cytoplasm
BfmR
Lon
Phage replication
Loki vulnerability factor
anti-Loki defense factor
B
BfmRS deficiency
Capsule structural change
Capsule loss
Resistance
C
BfmRS hyperactivation
LOS OC mutant
Lon mutant
Hypersusceptibility